SPECIAL MERRA COLLECTION

MERRA: NASA's Modern-Era Retrospective Analysis for Research and Applications

MICHELE M. RIENECKER,* MAX J. SUAREZ,* RONALD GELARO,* RICARDO TODLING,* JULIO BACMEISTER,*,+,## EMILY LIU,*,# MICHAEL G. BOSILOVICH,* SIEGFRIED D. SCHUBERT,* LAWRENCE TAKACS,*,# GI-KONG KIM,* STEPHEN BLOOM,*,# JUNYE CHEN,*,@ DOUGLAS COLLINS,*,# AUSTIN CONATY,*,# ARLINDO DA SILVA,* WEI GU,*,# JOANNA JOINER,& RANDAL D. KOSTER,* ROBERT LUCCHESI,*,# ANDREA MOLOD,*,@ TOMMY OWENS,*,# STEVEN PAWSON,* PHILIP PEGION,*,#,@@ CHRISTOPHER R. REDDER,*,# ROLF REICHLE,* FRANKLIN R. ROBERTSON,** ALBERT G. RUDDICK,*,# META SIENKIEWICZ,*,# AND JACK WOOLLEN++

* *Global Modeling and Assimilation Office, NASA Goddard Space Flight Center, Greenbelt, Maryland*
+ *Goddard Earth Sciences and Technology Center, University of Maryland, Baltimore County, Baltimore, Maryland*
# *Science Applications International Corporation, Beltsville, Maryland*
@ *Earth System Sciences Interdisciplinary Center, University of Maryland, College Park, College Park, Maryland*
& *Atmospheric Chemistry and Dynamics Branch, NASA Goddard Space Flight Center, Greenbelt, Maryland*
** *NASA Marshall Space Flight Center, Huntsville, Alabama*
++ *NOAA/National Centers for Environmental Prediction, Camp Springs, Maryland*

(Manuscript received 4 January 2011, in final form 18 March 2011)

ABSTRACT

The Modern-Era Retrospective Analysis for Research and Applications (MERRA) was undertaken by NASA's Global Modeling and Assimilation Office with two primary objectives: to place observations from NASA's Earth Observing System satellites into a climate context and to improve upon the hydrologic cycle represented in earlier generations of reanalyses. Focusing on the satellite era, from 1979 to the present, MERRA has achieved its goals with significant improvements in precipitation and water vapor climatology. Here, a brief overview of the system and some aspects of its performance, including quality assessment diagnostics from innovation and residual statistics, is given.

By comparing MERRA with other updated reanalyses [the interim version of the next ECMWF Re-Analysis (ERA-Interim) and the Climate Forecast System Reanalysis (CFSR)], advances made in this new generation of reanalyses, as well as remaining deficiencies, are identified. Although there is little difference between the new reanalyses in many aspects of climate variability, substantial differences remain in poorly constrained quantities such as precipitation and surface fluxes. These differences, due to variations both in the models and in the analysis techniques, are an important measure of the uncertainty in reanalysis products. It is also found that all reanalyses are still quite sensitive to observing system changes. Dealing with this sensitivity remains the most pressing challenge for the next generation of reanalyses.

Production has now caught up to the current period and MERRA is being continued as a near-real-time climate analysis. The output is available online through the NASA Goddard Earth Sciences Data and Information Services Center (GES DISC).

1. Introduction

Reanalyses combine model fields with observations distributed irregularly in space and time into a spatially complete gridded meteorological dataset, with an unchanging model and analysis system spanning the historical data record. The earlier generations of reanalyses from the National Oceanic and Atmospheric Administration/National Centers for Environmental Prediction (NOAA/NCEP), the European Centre for Medium-Range Weather

Current affiliation: National Center for Atmospheric Research, Boulder, Colorado.

@@ Current affiliation: NOAA/Earth Systems Resource Laboratory, Boulder, Colorado.

Corresponding author address: Michele Rienecker, Global Modeling and Assimilation Office, Code 610.1, NASA Goddard Space Flight Center, Greenbelt, MD 20771.
E-mail: michele.m.rienecker@nasa.gov

DOI: 10.1175/JCLI-D-11-00015.1

© 2011 American Meteorological Society

Forecasts (ECMWF), and the Japan Meteorological Agency (JMA) (e.g., Kalnay et al. 1996; Uppala et al. 2005; Onogi et al. 2005) have proven to be extremely valuable scientific tools, enabling climate and weather research not otherwise possible. They continue to be used, even with their known limitations, because of the basic utility afforded by such datasets for scientific analysis.

The Modern-Era Retrospective Analysis for Research and Application (MERRA) was stimulated by the recognition that various aspects of the hydrologic cycle represented in previous generations of reanalyses were not adequate for climate and weather studies. MERRA proposed to improve upon the water cycle as a contribution to the science community and to reanalysis research. MERRA's span of most of the satellite era is also intended to place observations from NASA's Earth Observing System (EOS) satellites, particularly those available since October 2002 from EOS/*Aqua*, into a climate context.

MERRA was generated with version 5.2.0 of the Goddard Earth Observing System (GEOS) atmospheric model and data assimilation system (DAS). The system, the input data streams and their sources, and the observation and background error statistics are documented fully in Rienecker et al. (2008, henceforth R2008). Unlike the atmospheric reanalyses from centers focused on operational weather prediction, the GEOS atmospheric DAS was developed with NASA instrument teams and the science community as the primary customers. Hence, the performance drivers of the GEOS DAS products have historically been temperature and moisture fields suitable for the EOS instrument teams, wind fields for the transport studies by the stratospheric and tropospheric chemistry communities, and climate-quality reanalyses (Schubert et al. 1993).

This paper provides an introduction to MERRA for a series of papers that evaluate the MERRA products and their uses in particular scientific investigations. It summarizes the DAS and provides some technical details as well as providing some insights into the system's performance. Other papers in the series analyze various aspects of the scientific quality of MERRA. For example, Bosilovich et al. (2011) evaluate MERRA from an energy and water budget perspective; Robertson et al. (2011) analyze the effects of the changing observing system on MERRA's energy and water fluxes; Schubert et al. (2011) highlight the usefulness of MERRA for characterizing the nature and forcing of short-term climate extremes, such as heat waves and flooding events; and R. I. Cullather and M. G. Bosilovich (2011, unpublished manuscript) and Cullather and Bosilovich (2011) evaluate MERRA surface fields in the polar regions. Reichle et al. (2011, manuscript submitted to *J. Climate,* hereafter referred to as R2011) evaluates MERRA land surface hydrological fields in offline tests and introduces a supplemental and improved set of fields. Yi et al. (2011) and Decker et al. (2011, manuscript submitted to *J. Climate*) evaluate surface meteorological forcing fields and surface fluxes over land from MERRA and other reanalyses with satellite estimates and in situ observations from flux towers. Roberts et al. (2011, manuscript submitted to *J. Climate*) and Brunke et al. (2011) analyze surface turbulent fluxes over the ocean from MERRA and other data products. Harnik et al. (2011) use MERRA to analyze decadal changes in downward wave coupling between the stratosphere and troposphere. By identifying both the strengths and weaknesses of the products, research efforts such as these provide valuable feedback that can improve future reanalyses.

Section 2 summarizes the DAS and processing strategy for MERRA. Section 3 summarizes the observations used and provides some details on the processing of radiosondes and satellite radiances. An evaluation of the status of the spinup for several fields is provided in section 4. Innovation statistics, as one measure of the quality of MERRA, are discussed in section 5. Sections 6–8 provide a view of how MERRA and other recent reanalyses have improved upon earlier generations. Remaining challenges are also discussed. Section 9 provides information about MERRA products and how they can be accessed. Finally, section 10 looks ahead to the next generation of reanalyses. A list of the acronyms and their definitions is provided in appendix A.

2. The MERRA system and production

a. The GEOS-5 Data Assimilation System

The GEOS-5 atmospheric general circulation model (AGCM) used for MERRA is based on finite-volume dynamics (Lin 2004) found to be effective for transport in the stratosphere (e.g., Pawson et al. 2007). It includes moist physics with prognostic clouds (Bacmeister et al. 2006), a modified version of the relaxed Arakawa–Schubert convective scheme described by Moorthi and Suarez (1992), the shortwave radiation scheme of Chou and Suarez (1999), and the longwave radiation scheme of Chou et al. (2001). Two atmospheric boundary layer turbulent mixing schemes are used. The Louis et al. (1982) scheme is used in stable situations with no planetary boundary layer (PBL) clouds, while the Lock et al. (2000) scheme is used for unstable or cloud-topped PBLs. GEOS-5 incorporates both an orographic gravity wave drag scheme based on McFarlane (1987) and a scheme for nonorographic waves based on Garcia and Boville (1994). The land surface is modeled with the Catchment Land Surface Model (Koster et al. 2000). The grid used for

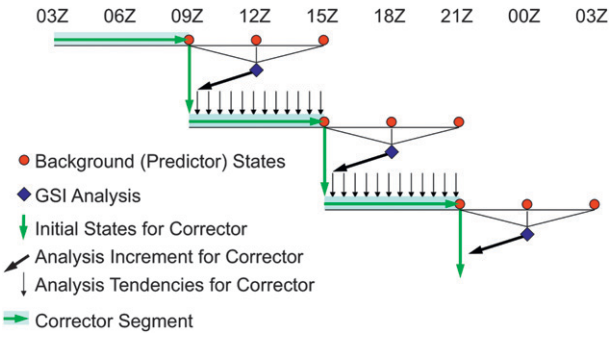

FIG. 1. A schematic of the IAU implementation in GEOS-5.

MERRA is ½° latitude × ⅔° longitude with 72 vertical levels, from the surface to 0.01 hPa. Additional details are provided in R2008.

MERRA uses a three-dimensional variational data assimilation (3DVAR) analysis algorithm based on the Gridpoint Statistical Interpolation scheme (GSI; Wu et al. 2002; Derber et al. 2003; Purser et al. 2003a,b) with a 6-h update cycle. The GSI, originally developed at NCEP and now jointly developed by NCEP and the GMAO, includes a number of advancements over 3DVAR algorithms used previously. In particular, the observation-minus-background departures are computed with greater temporal accuracy, and a dynamic constraint on noise is employed to improve the balance properties of the analysis solution. Unlike CFSR, which also uses the GSI, GEOS-5 uses an incremental analysis update (IAU) procedure (Bloom et al. 1996) in which the analysis correction is applied to the forecast model gradually, through an additional tendency term in the model equations during the corrector segment (Fig. 1). This has ameliorated the spin-down problem with precipitation during the very early stages of the forecast and greatly improved aspects of the stratospheric circulation, especially the residual circulation, because of temporally smoother transport.

MERRA, like other current reanalyses, makes extensive use of satellite radiance information, including data from hyperspectral instruments such as the Atmospheric Infrared Sounder (AIRS) on *Aqua*. The assimilation of radiance data requires a forward radiative transfer model (RTM) as the observation operator, to calculate the model-equivalent radiances, and the corresponding Jacobian to calculate the influences in model space of the radiance increments calculated from the analysis. For this, the GSI is coupled to the Community Radiative Transfer Model (CRTM; Han et al. 2006; Chen et al. 2010). The CRTM employs the compact version of Optical Path Transmittance (OPTRAN) (McMillin et al. 2006) for its gaseous absorption model. Saunders et al. (2007) compare the performance (forward model, transmittance, and Jacobians) of several RTMs for AIRS channels. Both OPTRAN version 7 (an earlier version of OPTRAN) and the Radiative Transfer for TIROS Operational Vertical Sounder model, version 7 (RTTOV-7), which is used in other operational analyses, were consistently in the set of good performers, agreeing to within 0.02 K to a reference line-by-line model for most channels. Chen et al. (2010) show that the forward models have biases of less than 0.1 K for microwave channels.

The CRTM was used for all radiance data except the Stratospheric Sounding Unit (SSU). The forward model for SSU has to take into account a leaking problem in the instrument's CO_2 cell pressure modulator that caused the radiances from each satellite to drift in time (Kobayashi et al. 2009). Since this information was not available in the CRTM at the time of MERRA development, the radiative transfer calculations for the SSU used an external module that incorporated the cell pressure information and was integrated into the GSI outside the CRTM. Shine et al. (2008) shows that the SSU spectral weighting functions are also sensitive to changes in atmospheric CO_2 concentrations; however, this information was not included in the forward model used for MERRA.

Since no land surface analysis was attempted, MERRA land surface estimates reflect the catchment model's time integration of the surface meteorological conditions (precipitation, radiation, wind speed, etc.) generated by the AGCM during the corrector segment.

b. *Boundary and ancillary data*

Unlike more recent versions of the GEOS-5 system, the MERRA AGCM uses a climatological aerosol distribution generated using the Goddard Chemistry, Aerosol, Radiation, and Transport (GOCART) model with transport based on a previous (GEOS-4) version of the AGCM (Colarco et al. 2010). The MERRA AGCM does, however, use the analyzed ozone generated by the DAS. The sea surface temperature and sea ice concentration boundary conditions are derived from the weekly 1° sea surface temperature product of Reynolds et al. (2002), linearly interpolated in time to each model time step. The MERRA system also nudges the stratospheric water vapor to zonal-mean climatological values based on data from the Halogen Occultation Experiment (HALOE; Randel et al. 1998) and the Microwave Limb Sounder (MLS) on the *Aura* satellite.

c. *Production*

MERRA was processed in three separate streams, each spun up in two stages: a 2-yr analysis at 2° × 2.5° and then a 1-yr analysis on the MERRA grid. Unfortunately, some system changes were made between spinup and production; these included small changes to the model that should have had little impact on the analysis, but also

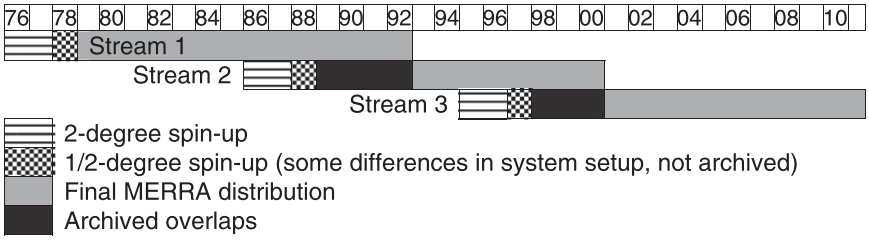

FIG. 2. The MERRA production streams, showing the original spinups, the overlaps, and the final MERRA distribution.

updates to the spectral coefficients used in the CRTM and a correction to the quality control of the microwave observations. Since the spinup was primarily aimed at the root-zone soil moisture, it was felt that these changes would not impede spinup. However, streams 1 and 2 were each extended to overlap the next stream so that the overlaps could be used to examine the adequacy of the spinup procedure and to quantify the uncertainty in individual fields. The adequacy of the spinup is discussed in section 4. The final MERRA distribution is from stream 1 for 1 January 1979–31 December 1992, followed by stream 2 for 1 January 1993–31 December 2000, and then continues with stream 3 for 1 January 2001–present. Hence, the distributed product segments from streams 1–3 have been spun up for 0, 4, and 3 yr, respectively, at MERRA resolution with the precise MERRA system configuration (Fig. 2). With the overlaps complete, and stream 3 now at ''the present,'' data production is being continued as a near-real-time climate analysis from stream 3 alone.

3. Observations

The various data types used in MERRA and the timeline of their availability are summarized in Fig. 3. The complete listing of the data streams and their sources are provided in appendix B. The quality control procedures, the channels used for radiance assimilation, and the observation error characteristics are presented in R2008.

MERRA benefited from the observational assembly for the NCEP–NCAR reanalysis, the NCEP preparations for its latest reanalysis, the CFSR (Saha et al. 2010), and also advances made for the interim (1989–present) version of the next ECMWF Re-Analysis (ERA-Interim; Dee and Uppala 2009, henceforth DU09). While the datasets used in MERRA, ERA-Interim, and CFSR are similar, there are some known differences in the observations and their processing, as mentioned below. Obviously, these differences can be one source of differences between the various reanalysis products; other sources are the model and the analysis methods that were used.

Figure 4a shows the total number of observations available for assimilation and their breakdown by instrument or type. Each separate channel is counted for the radiance data and each separate level and data type for other observations. A large increase in the number of observations is seen with the availability of the Advanced TIROS Operational Vertical Sounder (ATOVS) in 1998, and then again with the availability of AIRS and the Advanced Microwave Sounding Unit-A (AMSU-A) on the *Aqua* satellite in 2002. After 2002, roughly 4 million observations are considered in each 6-h analysis cycle, with roughly half of these being assimilated (Fig. 4b) because of quality control checks as well as data thinning.

a. Conventional observations

Conventional observations, that is, nonradiance data, consist of measurements of standard atmospheric variables (i.e., pressure, temperature, height, wind components) taken by instrumentation on weather stations, balloons, aircraft, ships, buoys, and satellites. A fairly complete global coverage pattern of these observations has been available since roughly the late 1940s. The NCEP–NCAR reanalysis (Kistler et al. 2001) assimilated these data starting in 1948, as did ERA-40, starting in 1958. Archives of conventional observations were preserved among a number of national, academic, and military sources worldwide. Institutions such as NCAR and

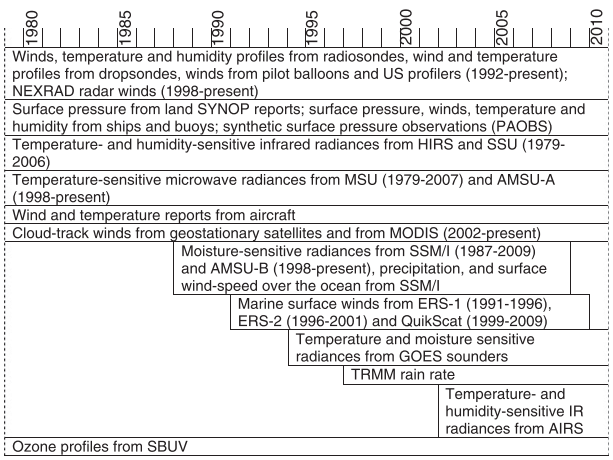

FIG. 3. Summary of the observing system used for MERRA.

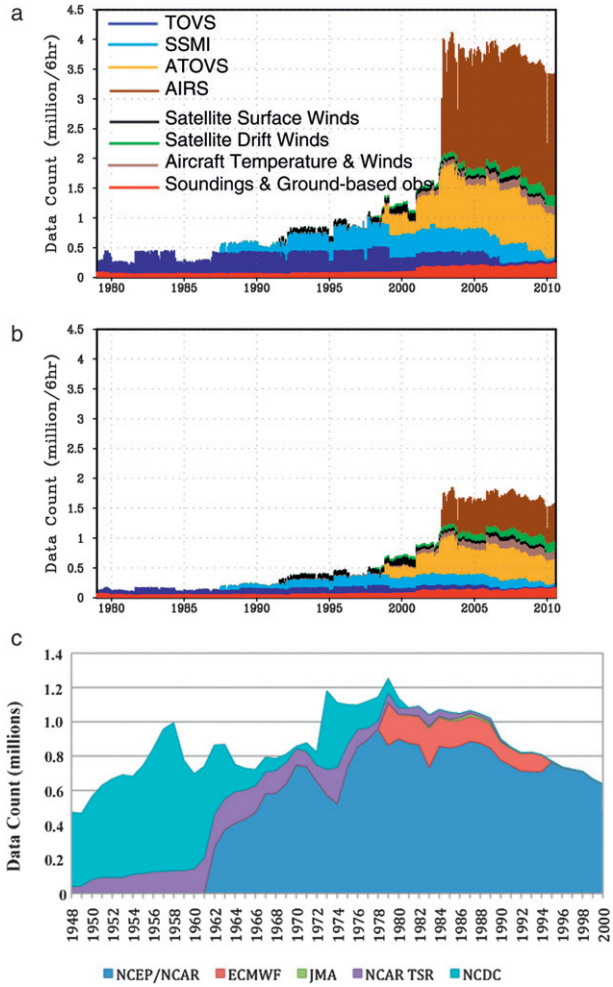

FIG. 4. Time series of (a) the number (millions) and types of observations considered for assimilation during a 6-h window, and (b) those observations actually assimilated. (c) Counts of merged radiosonde soundings per year from each major archive source, 1948–2000.

the National Climatic Data Center (NCDC) have collected and converted many of the original archives into digital formats compatible with modern data processing systems. To produce homogeneous sets of observations for use in reanalysis, it is necessary to combine observations from the different sources, eliminating redundant information in the process. This was done for all the conventional data types listed above. Figure 4c illustrates the number of radiosonde soundings per year from each major source archive represented in the composited set of radiosondes produced for reanalysis, 1948–2000. An itemization of all source files from each archive for each conventional data type is given in appendix B.

Radiosonde data remain some of the most important observations for meteorological analyses. MERRA used radiosonde data that were quality controlled by NCEP for CFSR, with additional processing and correction of the data undertaken at GMAO. Corrections included the removal of large time-mean temperature differences in radiosonde observations collected at 0000 and 1200 UTC with the Vaisala RS-80 instrument (from 1994 onward). The differences occur as a result of a coding error in the postprocessing software at the observing stations that primarily affects observations in the stratosphere (Redder et al. 2004). The reported elapsed time archived in the NCDC database was used to undertake the corrections. The homogenization scheme of Haimberger (2007), the Radiosonde Observation Bias Correction Using Reanalysis (RAOBCORE) version 1.4, was then applied to radiosonde observations until 2005, with updated values consistent with the Vaisala RS-80 corrections. After these corrections were made to the radiosonde temperature observations, a radiation bias correction was applied according to the NCEP radiation correction (RADCOR) tables (Collins 1999; Ballish and Kumar 2008), but only to account for seasonal changes in the solar elevation angle that affect the thermistor. The ERA-40 blacklist was used for the entire duration of the reanalysis. The other conventional observations used for MERRA are listed in appendix B (see Table B1).

b. *Satellite radiance data and variational bias correction*

MERRA, like other current reanalyses, makes extensive use of satellite radiance data from both operational and research instruments (see Table B3). Successful use of radiance data requires careful quality control and bias correction procedures that are channel specific. The bias in a given satellite channel can vary significantly in space and time depending on the atmospheric conditions, systematic errors in the radiative transfer model, and quality and age of the instrument. In most data assimilation schemes, the bias in each satellite radiance measurement is represented by a linear predictor model with a relatively small number (~10) of parameters. In the earlier reanalyses that used satellite radiances, including ERA-40 (Uppala et al. 2005) and the Japanese 25-yr Reanalysis (JRA-25) (Onogi et al. 2005), these parameters were estimated separately for each channel using an offline procedure based on a reference dataset.

In the current reanalyses, bias estimation is performed during the data assimilation procedure. The satellite scan-angle-dependent bias is estimated directly as an exponential moving average filter of the innovations for brightness temperatures, with the most recent estimate given low weight so that the bias estimate evolves slowly (Saha et al. 2010, and the supplemental material available online). The airmass-dependent bias is estimated using a variational bias correction scheme (VBC) in which the

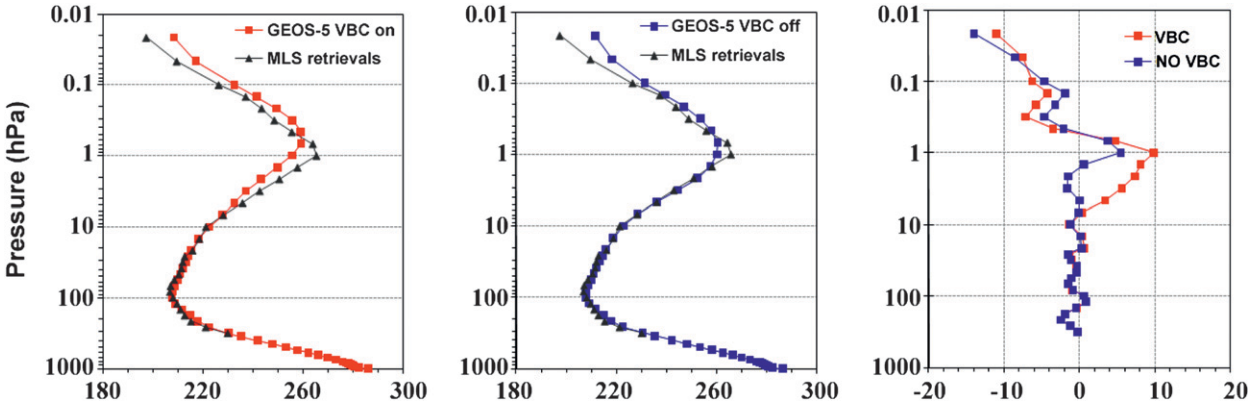

FIG. 5. Mean temperature profiles (K) from MLS and collocated MERRA profiles over the globe for August 2008. Comparisons (left) when VBC is applied to AMSU-A channel 14 and (middle) when VBC is omitted, and (right) the differences between the mean profiles for each case.

bias parameters are updated during each analysis cycle by including them in the control vector used to minimize the analysis cost function (Derber and Wu 1998; Dee 2005). This ensures that the bias estimates are continuously adjusted to maintain the consistency of the bias-corrected radiances with all other information used in the analysis, including conventional observations and the model background state. An important technical advantage of this approach is that it removes the need for manual tuning and other interventions as the satellite observing system changes over time. The bias estimates also adapt in response to natural phenomena that can severely affect the radiance measurements, such as the Mount Pinatubo eruption in 1991 (see Fig. 5 in DU09). The use of VBC thus represents one of the most important advances in the assimilation methodology of the current generation of reanalyses. The linear predictors used in the GSI differ slightly from those used for ERA-Interim and are documented in R2008.

As discussed in Saha et al. (2010, and the supplemental material available online) the initialization of the bias coefficients requires some care, especially the slowly evolving scan angle bias. For CFSR, an offline training period of 3 months was used to spin up the bias coefficients prior to their use in the reanalysis. For MERRA, offline training periods were also used; with the training period varying from 1 to 6 months depending on the testing that was being conducted to finalize the system. Since the stabilization of the cloud liquid water bias correction term for AMSU-A was found to take at least 1 yr, this term was initialized from a test system that had been running for longer than that.

Not all instrument channels can be bias corrected using the assimilation machinery of VBC. The success of such corrections depends entirely on having either an AGCM with low biases or other observations with low biases to provide an anchor for the analysis. Since models tend to have large biases in the upper stratosphere and mesosphere, and there are no observations consistently available over the entire reanalysis period, bias correction for instrument channels with weighting functions that extend above about 2 hPa is problematic.

An evaluation of the MERRA temperature fields in the upper stratosphere, as well as the impacts of trying to bias correct those high-peaking channels, is provided by a comparison with temperature data from MLS (Fig. 5). MLS provides detailed temperature structure from about 316 hPa to about 0.001 hPa (Manney et al. 2008b). These data were not assimilated in MERRA, providing independent validation. For the comparison shown in Fig. 5, approximately 95 000 MLS profiles were collocated to the MERRA grid during August 2008. The right-hand panel in Fig. 5 shows that the analysis has a cold bias of up to 10 K from about 10 to 0.8 hPa when VBC was activated for channel 14 on the AMSU-A. Without VBC, this channel effectively corrects the model bias, which is responsible for the analysis bias when VBC is activated. Accordingly, in MERRA, VBC is not applied to AMSU-A channel 14 or SSU channel 3 [which peaks at a similar level, about 1.5 hPa (Kobayashi et al. 2009)]. However, biases of up to 5 K are still evident at 1 hPa and above.

Just as variational bias correction has provided significant benefit to the assimilation of satellite radiances, so too has the cross calibration of certain observation datasets improved their usefulness in the current reanalyses. The Microwave Sounding Unit (MSU) instruments on board TIROS-N and the NOAA series of satellites to *NOAA-14* provide one of the longest records of remotely sensed atmospheric temperature from a single sensor type, extending from 1978 to 2007, with overlapping lifetimes of up to 3 yr between satellites. In the original datasets, the global mean bias estimates for the same MSU channel on

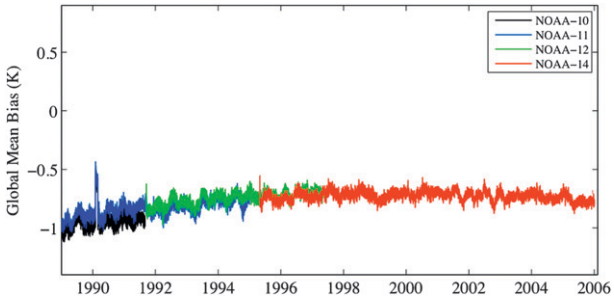

FIG. 6. Time series of MERRA's global mean 6-hourly variational bias estimates (K) for cross-calibrated MSU channel 2 radiance data from *NOAA-10*, *-11*, *-12*, and *-14*.

different satellites differ by up to 1 K or more (DU09), limiting the usefulness of these data for climate change research and possibly having a negative effect in the variational bias correction scheme. The National Environmental Satellite, Data, and Information Service (NESDIS) has begun recalibrating observations from MSU as well as other instruments using a simultaneous nadir overpass (SNO) method (Zou et al. 2006). The recalibrated radiances for MSU channels 2–4 on board *NOAA-10*, *-11*, *-12*, and *-14* have been assimilated in MERRA and exhibit near-uniform biases, albeit with a discernible trend over the first few years of the data record (Fig. 6). The bias estimates shown here may be compared with those of the uncalibrated radiances used in ERA-Interim (DU09, their Fig. 3). Zou et al. (2006) estimate the new global ocean-averaged intersatellite biases for channel 2 to be between 0.05 and 0.1 K. The VBC procedure used in MERRA, which includes all other available observations as well as information from the model background state, is consistent with that and is much smaller than the ~1.5-K intersatellite bias from the raw measurement (DU09). Note that it has not been determined yet whether cross calibration affects the quality of the reanalysis product, but it is reasonable to speculate that it is beneficial to the performance of the VBC.

4. Evaluation of the spinup

The primary fields for which spinup of the assimilation system is a concern are the land surface states and the stratosphere. The spinup of the stratosphere is addressed elsewhere (S. Pawson et al. 2011, unpublished manuscript, hereafter P2011); here, we examine the troposphere, the land surface states, and precipitation. The tropospheric meteorological fields [as assessed by the root-mean-square (RMS) difference in 500-hPa height during the overlap periods] reached a steady state after about 1.5 yr of spinup with the final MERRA configuration (Fig. 7a). Precipitation takes slightly longer, about 2 yr (Fig. 7b). The long time scale required for the decay of the RMS

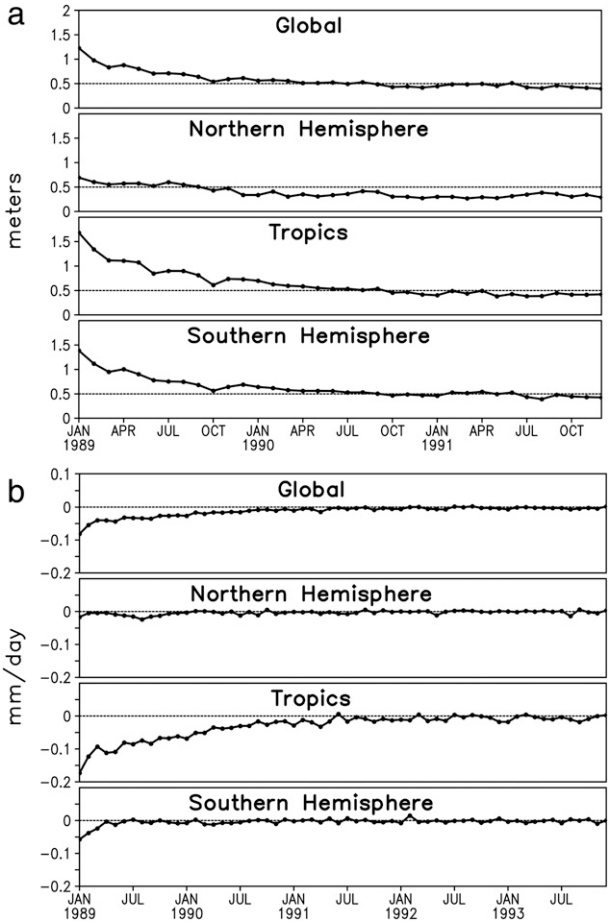

FIG. 7. Time series of (a) RMS difference in monthly mean 500-hPa height (m) and (b) difference in monthly mean precipitation (mm day^{-1}) from the overlap of streams 1 and 2. Stream 2 was initialized at the MERRA resolution in January 1988 after a 2-yr spinup on a 2° × 2.5° grid. The tropical band covers 15°S–15°N.

differences is due, at least in part, to the time needed for the satellite bias corrections to stabilize to the same value. This in turn will be affected by slight differences in the choice of observations to be assimilated, since both data selection and quality control rely on the background fields used for analysis. However, the initial differences in the overlaps are roughly an order of magnitude less than the differences between analyses from different systems (see, e.g., the MERRA atlas described in section 9). They are also less than 0.05% of the height itself and less than 0.5% of the variation of the field across the globe.

Subsurface properties, such as the root-zone soil wetness shown in Fig. 8, reach their asymptote slightly more slowly, after a sharp drop in differences over the first 6 months of the overlap using the same model parameters (from 1 January 1989 in stream 2; see Fig. 8). Although the RMS differences in the Northern Hemisphere are

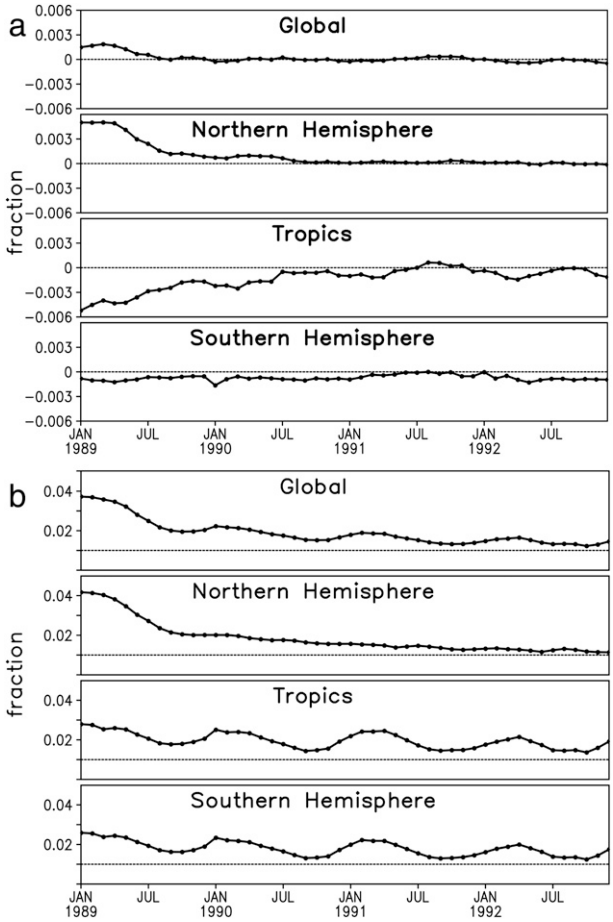

FIG. 8. Time series of the (a) mean and (b) RMS difference between streams 1 and 2 for monthly mean root-zone soil wetness (dimensionless fraction of saturated conditions, varying from 0 to 1). The tropical band covers 15°S–15°N.

still diminishing after 4 yr, they appear to reach a predictability limit, especially in the tropics and Southern Hemisphere where the RMS differences also display some seasonality. This seasonality appears to be related to the corresponding seasonality in the RMS differences in precipitation (not shown), which are presumably, in turn, related to the seasonal cycle of precipitation over tropical land. The maps of root-zone soil wetness differences for February (Fig. 9) show that the slowly decaying systematic differences tend to be in the high latitudes, where adjustments to soil moisture by evaporation or runoff cannot occur over long periods of the year because of frozen conditions.

5. Evaluation of MERRA through innovation statistics

The differences between the observations and the forecast background used for the analysis (the innovations or O-F for short) and those between the observations and the final analysis (O-A) are by-products of any assimilation system and provide information about the quality of the analysis and the impacts of the observations. Innovations have been traditionally used to diagnose observation, background, and analysis errors at observation locations (Hollingsworth and Lönnberg 1989; Dee and da Silva 1999). At the most simplistic level, innovation variances can be used as an upper bound on background errors, which are, in turn, an upper bound on the analysis errors. With more processing (and the assumption of optimality), the O-F and O-A statistics can be used to estimate observation, background, and analysis errors (Desroziers et al. 2005). They can also be used to estimate the systematic and random errors in the analysis fields. Unfortunately, such data are usually not readily available to users of reanalysis products. With MERRA, however, a gridded version of the observations and innovations used in the assimilation process is being made available. The dataset allows the user to conveniently perform investigations related to the observing system and to calculate error estimates.

The evolution of the mean and RMS of O-F and hemispheric data counts for assimilated surface pressure observations is shown in Fig. 10. In both hemispheres the RMS decreases slightly in time with the increasing number of observations. The large increase in observations in January 2001 reflects the introduction of METAR surface pressure observations into the assimilation. At the end of the period, the RMS values for both hemispheres are about 0.2 hPa greater than those from ERA-Interim (Dee et al. 2011a).

The mean O-F and O-A statistics for January 2004 radiosonde temperature observations at different pressure levels are shown for the globe and for the Arctic (north of 70°N) in Fig. 11. The global analysis biases are relatively small (less than 0.2 K) at most levels, with a cold bias (positive O-A) in the PBL and a warm bias in the upper troposphere, consistent with the analysis biases against independent MLS observations discussed earlier (Fig. 5). In the Arctic, both the model and analysis tend to be warmer than the observations, except close to the surface. The greater spread at lower levels in the Arctic region is presumably because of the seasonal influence of ice cover (e.g., Bromwich and Wang 2005).

Interestingly, these O-F statistics change with time (Fig. 12), especially in the upper troposphere. Since in the reanalysis the model does not change and there is no indication of degradation in the radiosonde observations themselves over time, we conclude that other observation types contribute to these changes in the agreement between the analysis (and also the background forecast) and the radiosondes. This issue is explored further in Fig. 13.

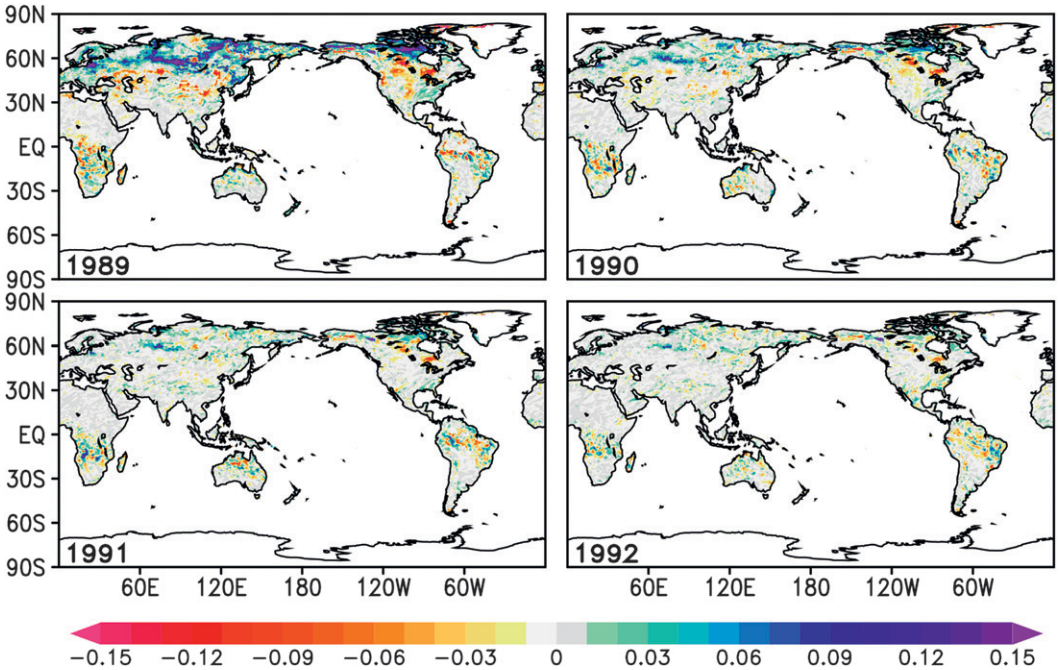

FIG. 9. The monthly mean difference between the root-zone soil wetness, stream 1 minus stream 2, for February 1989–92.

Even before the increase in the bias, there is a decrease in the standard deviation of the radiosonde innovations associated with the decrease in the number of radiosonde observations.

Figure 13a shows the time series of monthly innovation statistics for radiosonde temperatures at 300 hPa. The thin black line depicts the global mean of the monthly mean O-F for each month, smoothed with a 12-month running mean. Comparison with the same statistic for aircraft temperatures (Fig. 13b) shows that the increase in the magnitude of the upper-tropospheric bias with respect to radiosondes starting in the mid- to late 1990s coincides with an increase in aircraft observations, which have a warm bias (Cardinali et al. 2003; Ballish and Kumar 2008; DU09). As pointed out by DU09, after 1999 the mean analyzed temperatures near these altitudes are increasingly determined by the more numerous aircraft data, especially in the Northern Hemisphere, even though the observation error specified for radiosondes tends to be slightly lower than that specified for aircraft (0.65 K for radiosondes and 0.8 K for most aircraft observations at 300 hPa in MERRA).

Two complementary statistics are also depicted in Fig. 13. The red curve depicts the RMS of the O-F over both space and time for each month. The thick black line shows the spatial RMS of the gridded monthly mean values. The monthly mean of O-F should be close to zero if both the background and the observations are unbiased. The statistic for any single instrument will be nonzero because of biases in the background or because of the bias of a particular instrument relative to the other instruments used in the assimilation. If the mean O-F is small, the spatial RMS of the monthly mean (the thick black line) primarily reflects the large-scale structure of the background bias or possibly an inhomogeneity in the

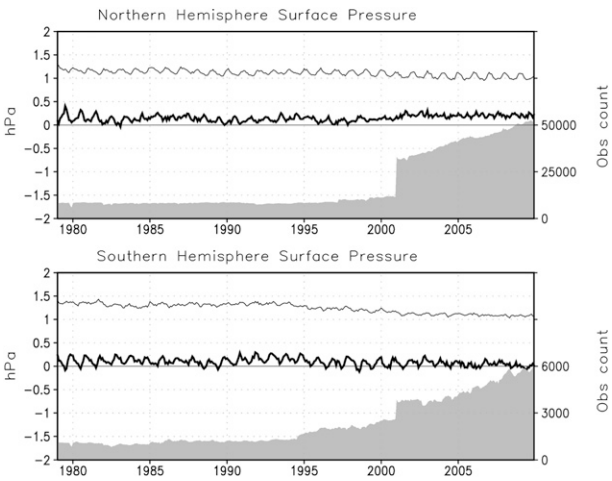

FIG. 10. Time series of the monthly mean (thick curve) and RMS (thin curve) of O-F residuals (hPa, left axis) for surface pressure observations in the (top) Northern and (bottom) Southern Hemispheres. The shaded curves indicate the monthly mean data counts (right axis) for each 6-h assimilation cycle.

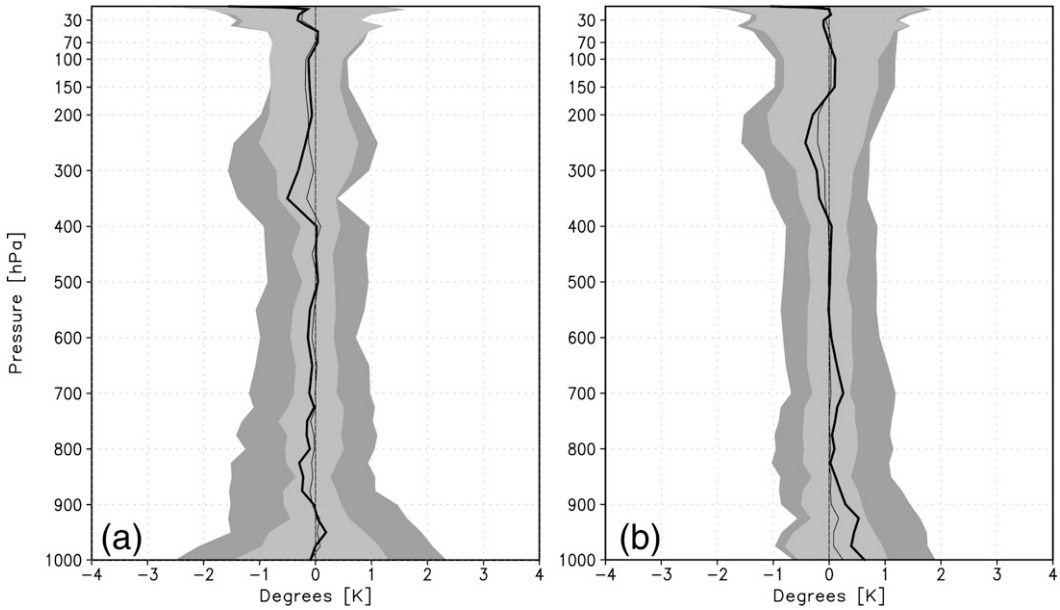

FIG. 11. The vertical profile of mean O-F (thick curve) and O-A (thin curve) residuals (K) for radiosonde temperature observations as a function of pressure level (hPa) during January 2004. The dark and light shading indicate ±1 standard deviation from the mean O-F and O-A values, respectively. (a) Global statistics and (b) statistics for the Arctic only.

observation distribution. Since, to a large part, the monthly mean removes the contribution of synoptic variability (i.e., the random component of the O-F), the difference between the red and thick black lines offers an indication of the contribution of synoptic-scale eddies to the O-F misfit. The closeness of the RMS statistics shown in Fig. 13 indicates that the dominant components of the background error are systematic rather than random.

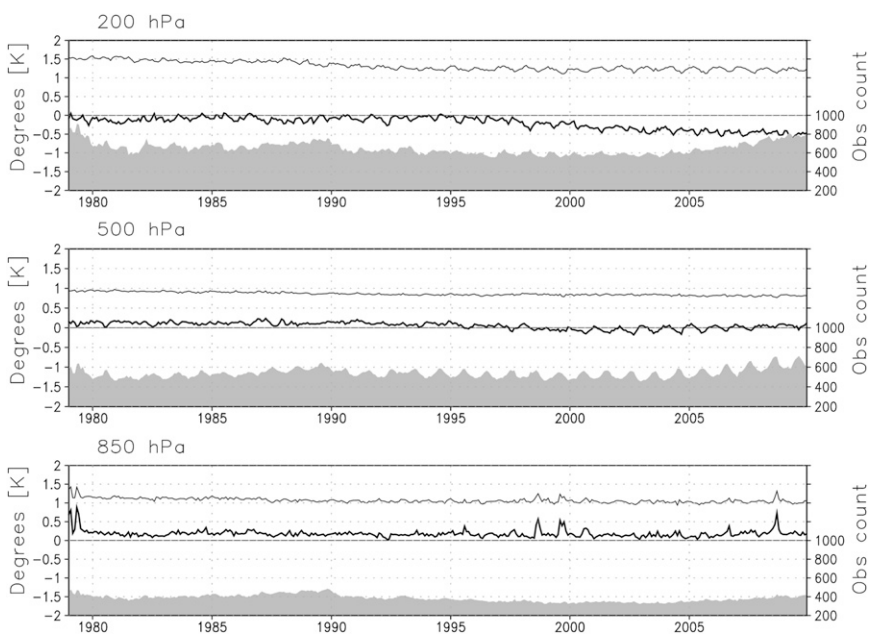

FIG. 12. Time series of the monthly global mean (thick curve) and RMS (thin curve) of O-F residuals (K, left axis) for radiosonde temperature observations at (top) 200, (middle) 500, and (bottom) 850 hPa. Negative mean values indicate that the observations are colder, on average, than the background. The shaded curves indicate the monthly mean data counts (right axis) for each 6-h assimilation cycle.

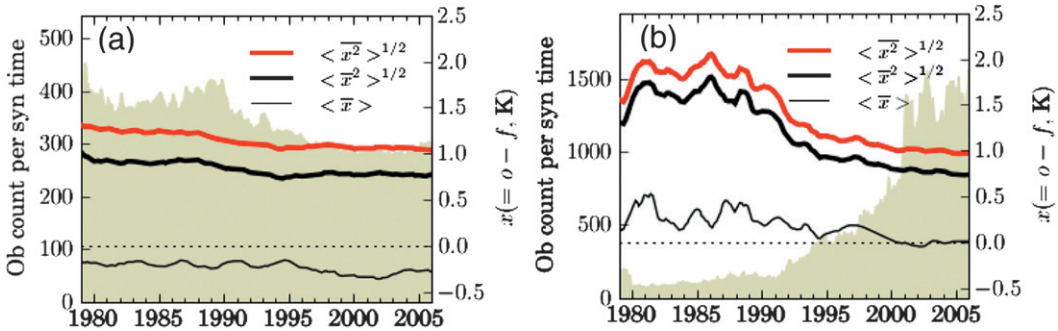

FIG. 13. (a) Time series of monthly global mean O-F statistics for radiosonde temperature observations at 300 hPa. The thin black line shows the global mean of the monthly mean O-F, the thick black line shows the spatial RMS of the monthly mean O-F, and the red line shows the global RMS O-F for the month, all in K (right axis). The shading represents the number of observations per synoptic time (left axis). Curves have been smoothed with a 12-month running mean. (b) The same statistics for temperature observations at 300 hPa, but taken from aircraft.

With MERRA's gridded observation and innovation datasets, a wealth of information is available for examination of the quality of the analyses and how the different observations impact the analyses and interact with each other. Such examinations can be conducted regionally or globally and should provide useful information for the next generation of reanalyses.

6. Climate variability

Many aspects of the quality of MERRA products are presented in other papers mentioned in section 1. In the next three sections, we touch on just a few fields that highlight improvements over earlier-generation reanalyses and on some of the issues that will still need to be addressed in the next generation.

One of the strengths of the most recent reanalyses is in their representation of interannual variability of the atmospheric state on monthly to seasonal time scales. However, the quality of the climate signal depends on both the variable and the area of interest. Not surprisingly, the interannual variability in analyzed fields, like 500-hPa height (not shown), from different reanalyses in the satellite era is almost indistinguishable. Perhaps more surprising is the agreement in higher-order moments, such as large-scale atmospheric transports, or in some of the derived fields, such as vertical velocity. The latter is illustrated in Fig. 14 by comparing results from MERRA and ERA-Interim. The difference in the representations of these climate anomalies, as indicated by the difference between monthly mean analyses for two different years [one a neutral year in terms of the El Niño–Southern Oscillation (ENSO) and one an El Niño year], is much smaller than the amplitude of the El Niño climate signal itself. This agreement is an improvement upon what was already a high level of agreement with the older ERA-40.

Figure 15 shows the zonal mean values of the interannual correlations between monthly mean quantities from MERRA and ERA-Interim, and between MERRA and selected observational datasets, for various quantities during January and July. While the correlations are generally high for dynamical variables such as tropospheric winds and eddy height (Fig. 15, top), they are considerably lower for thermodynamic and cloud-related variables such as precipitation and outgoing longwave radiation (OLR) (Fig. 15, bottom). The most challenging region for all quantities is obviously the tropics, more so for the near-surface winds than for the upper-tropospheric winds. The higher correlations between MERRA and ERA-Interim for precipitation and OLR, compared with the correlations between MERRA and the Global Precipitation Climatology Project (GPCP; Adler et al. 2003) or MERRA and the NOAA OLR product, emphasize the fact that the reanalyses are still more like each other than they are like the observational estimates.

The quality of the analyzed variability on longer time scales can be assessed through the time series of global mean interannual temperature anomalies in the troposphere and upper stratosphere (Fig. 16). Here, the comparison is made to ERA-Interim. Because of the notable changes over time in MERRA's annual cycle in the upper stratosphere, the anomalies have been calculated relative to the annual cycle determined for 2000–10. In the lower troposphere, which is well constrained by radiosonde data, MERRA and ERA-Interim track each other closely, with a warming trend through to 200 hPa. At 200 hPa, the difference in the trends of the two analyses reflects the differences in the impacts of the aircraft temperatures, which, as mentioned above, are known to have a warm bias (Ballish and Kumar 2008). The bias in MERRA at that altitude is about 0.5 K (Fig. 12) while in ERA-Interim it

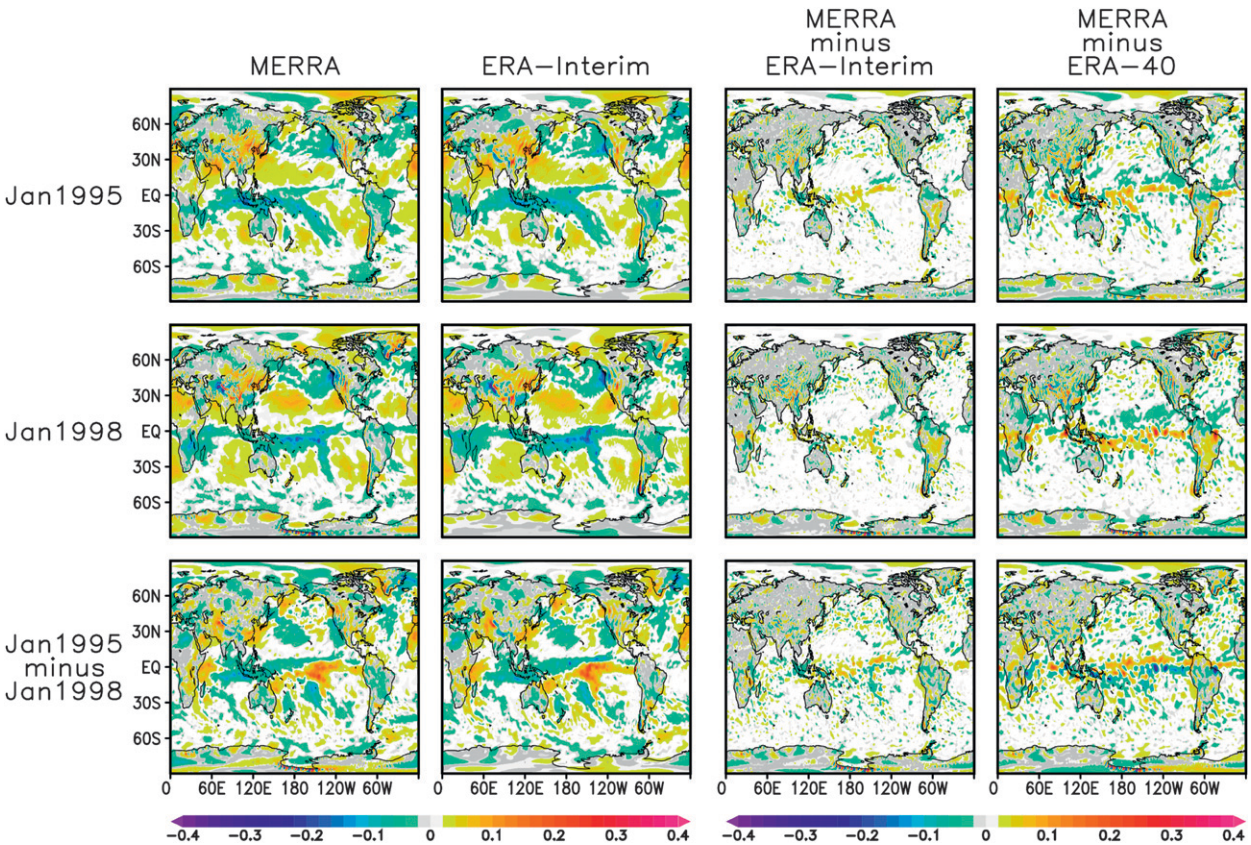

FIG. 14. The vertical velocity (Pa s^{-1}) at 500 hPa for (top) January 1995 and (middle) January 1998 from MERRA (first column) and ERA-Interim (second column). The differences between MERRA and ERA-Interim are shown in the third column while the fourth column compares MERRA with ERA-40. (bottom) The differences between the two years.

is about half that (DU09). So, although the anomalies at that height are almost indistinguishable from one another between 2000 and 2010, MERRA appears slightly cooler earlier and so has a slightly stronger trend. At 100 hPa, the MERRA anomalies are slightly warmer than those in ERA-Interim before 2000; otherwise, the interannual variations are highly correlated. Larger differences are apparent in the upper stratosphere. At 5 hPa and above, the high-peaking channels of AMSU-A introduce a discontinuity in ERA-Interim in late 1998, as discussed in detail by Dee and Uppala (2008) and Kobayashi et al. (2009). After that, the trends from both analyses from 1999 to 2010 agree very well at 5 and 10 hPa. The anomalies prior to 1999 are much stronger in MERRA than in ERA-Interim. This could possibly be related to the fact that the forward model used for MERRA did not include changes in atmospheric CO_2 concentrations in the SSU spectral weighting functions. A much more detailed discussion of MERRA fields in the stratosphere is provided in P2011.

7. Precipitation estimates

Bosilovich et al. (2011, hereafter referred to as B2011) examined the energy and water budgets in MERRA, and compared cloud and precipitation estimates from the latest reanalyses with the available observations. They used the precipitation from GPCP as the standard, but included the product from the Climate Prediction Center (CPC) Merged Analysis of Precipitation (CMAP) dataset (Xie and Arkin 1996) as a comparison to give some indication of the uncertainty in the observational products. The spatial correlation of the annual-mean precipitation from the analyses with the GPCP estimates (Fig. 17a) shows that the three new reanalyses are closer to the observations than previous products and are approaching the correlation between the two observational estimates. In addition to these improvements in the spatial distribution of precipitation, MERRA and ERA-Interim also show a marked decrease in its spatial variance (Fig. 17b), bringing them within the variance of the observational products. CFSR is somewhat higher, particularly in recent

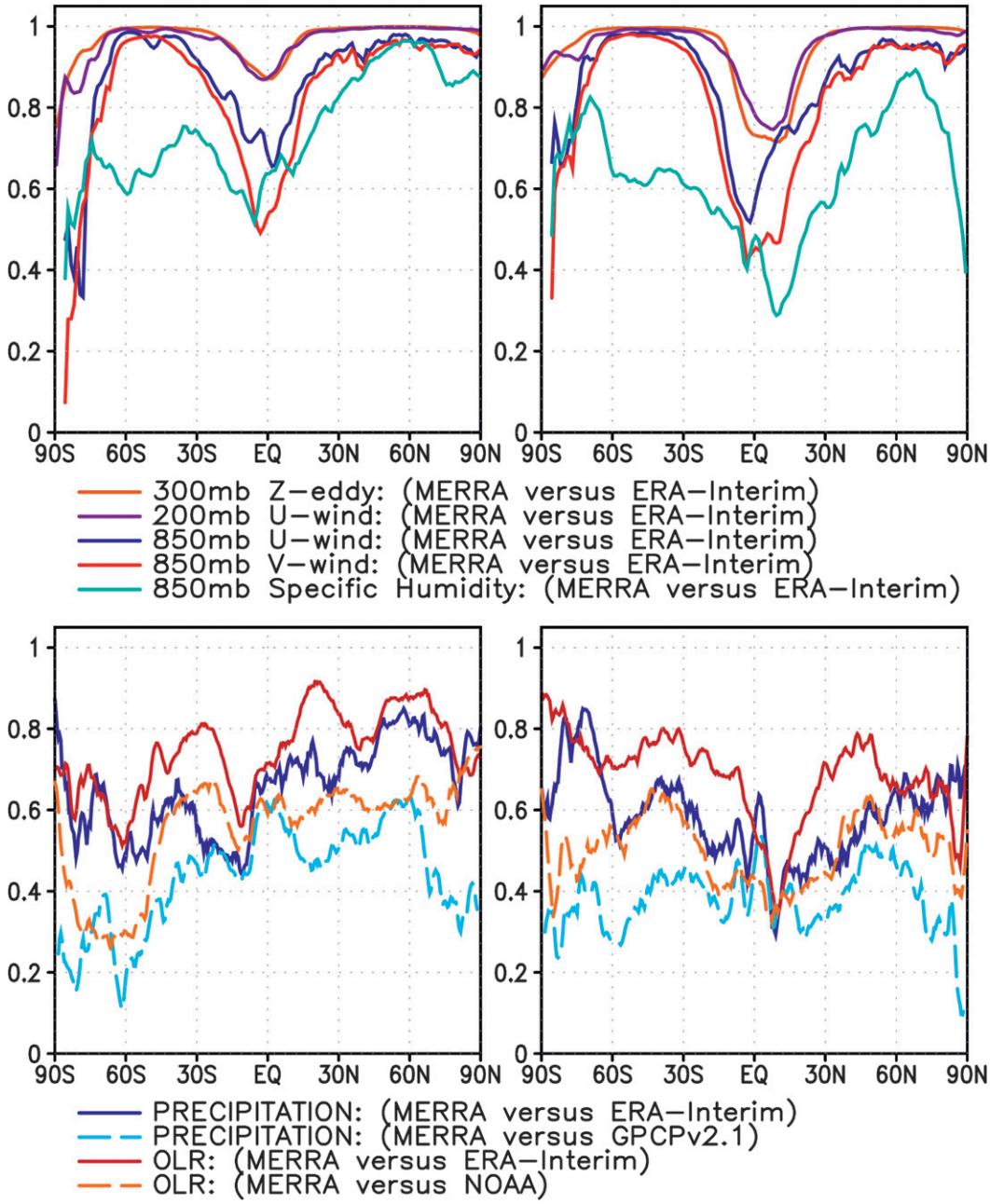

FIG. 15. Zonal-mean values of the correlation between MERRA and ERA-Interim, and between MERRA and selected observation datasets, for various monthly mean quantities during (left) January and (right) July for the period 1990–2008. Comparisons with GPCP precipitation and from NOAA's OLR product are also included.

years. Note that the variance from the NCEP–NCAR reanalysis (NR1) is also close to the observed, but with a poor spatial structure (Fig. 17a). In B2011, the improved agreement of the new reanalyses with the observed products is attributed to improvements over ocean regions, especially the tropical oceans.

It is important to point out that none of these reanalyses generates a precipitation analysis, that is, precipitation is not a control variable in the analysis procedure. Although microwave-retrieved rain-rate observations are assimilated in the GSI over ocean areas, these data are given a low weight and have only a weak impact on increments in temperature, specific humidity, and other control variables (Treadon et al. 2002). In sensitivity and tuning experiments conducted prior to MERRA production, the three-dimensional humidity observations [moisture-sensitive

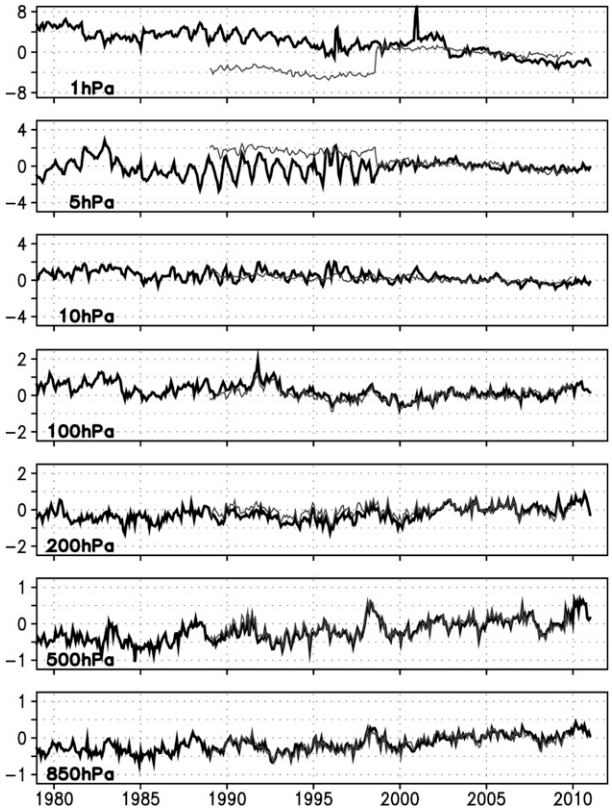

FIG. 16. Global-mean temperature anomalies from MERRA (thick line) and ERA-Interim (thin line). The anomalies have been computed relative to the 2000–10 annual cycle for each analysis. All calculations are based on monthly averaged fields.

radiance data from the Special Sensor Microwave Imager (SSM/I) and AMSU-B] were found to have a much larger impact on the precipitation than the precipitation observations themselves. Since the precipitation itself is not a control variable, in MERRA the precipitation product is stored from the ''corrector'' segment of the IAU cycle (see Fig. 1). The concatenation of these segments results in a single model run in which an extra tendency term, which changes at the end of each analysis cycle and accounts for the analysis increment, is added to each control variable. In this way, only the tendency of the state can have discontinuities and not the state itself. This significantly lowers the shock in precipitation that is experienced by systems that increment the state at the beginning of each analysis cycle. Ameliorating this shock is particularly important in 3DVAR systems such as GSI.

The precipitation distribution is obviously related to the precipitable water in the atmosphere. Figure 18 shows that MERRA and ERA-Interim display similar biases in the total column water vapor (TCWV) relative to the gridded SSM/I product of Ferraro et al. (1996). The bias patterns are very similar although MERRA has a larger negative bias in the southern high latitudes while ERA-Interim has a larger negative bias near the equator. The biases are lower than those in ERA-40 and are of opposite sign in the tropics. Interestingly, regions of positive bias in the midlatitudes are consistent across all three reanalyses (at least for this particular month). For comparison, Alishouse et al. (1990) used collocated radiosondes to estimate the RMS accuracy of SSM/I-derived TCWV over the ocean as approximately 2.4 kg m^{-2}. They estimated the bias in the tropics to be about the same level [$(-2.1, 0.5, 2.4)$ kg m^{-2} in the respective bands (20°S–0°, 0°–20°N, 20°–25°N)], and the bias in the higher latitudes to be less than 1 kg m^{-2} [$(0.6, -0.9, 0.8)$ kg m^{-2} in the respective bands (55°–25°S, 25°–55°N, 55°–60°N)].

a. Impacts of observing system changes on precipitation estimates

The time series of global monthly mean precipitation (Fig. 19) provides perhaps the clearest evidence that, despite the major advances, the latest reanalyses are still significantly impacted by changes in the observing system. There is a trend (or series of jumps and different trends) in MERRA associated with the introduction of

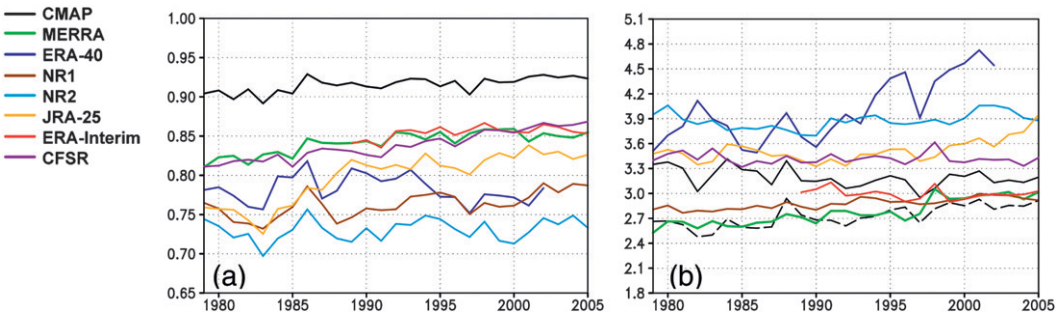

FIG. 17. (a) The time series of the spatial correlation of annual-mean precipitation averaged over the tropics (15°S–15°N, left-hand figure) from several reanalyses with that from GPCP. The comparison of CMAP against GPCP is also shown (black curve). (b) The annual-mean spatial standard deviation of precipitation (mm day^{-1}) over the tropics. The black dashed line denotes GPCP.

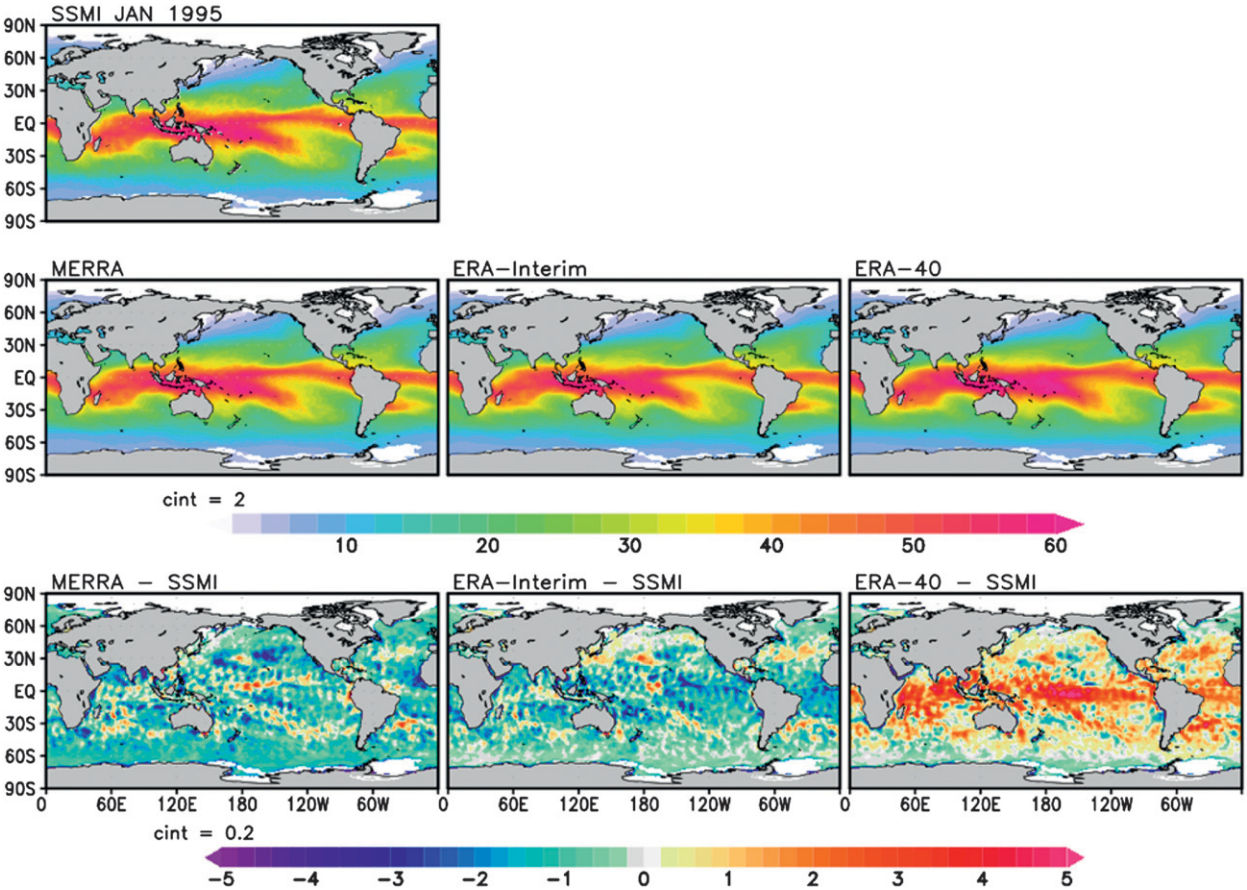

FIG. 18. Monthly mean total column water vapor (kg m^{-2}) for January 1995. (top) The observed field from the SSM/I product of Ferraro et al. (1996). (middle) MERRA (leftmost panel), ERA-Interim (center panel), and ERA-40 (rightmost panel) results. (bottom) The difference of the reanalyses from the SSM/I data.

SSM/I observations in July 1987 and of AMSU-A data from *NOAA-15* in November 1998. There is a clear indication (from experiments in which particular instruments or channels were withheld from the assimilation, also shown in Fig. 19) that the global precipitation in MERRA is sensitive to AMSU-A data, and in particular to the window channels, 1–3 and 15 (see Robertson et al. 2011 and the inset of Fig. 19). In contrast, ERA-Interim, which does not assimilate those window channels, is sensitive to the assimilation of SSM/I data (D. Dee 2010, personal communication).

The dates of changes in the availability of AMSU-A and SSM/I data, and in the rain-rate data from the TRMM Microwave Imager (TMI), are presented in Table 1. Matching these dates with notable changes in Fig. 19, it appears that MERRA responds more to AMSU-A than to SSM/I. Significant increases in precipitation are observed with the introduction of AMSU-A on *NOAA-15* in 1998 and *NOAA-16* in 2001, although there is little discernible impact from the introduction of a third AMSU-A on *NOAA-18* in 2005. The loss of AMSU-A on *NOAA-16* in 2008 coincides with a clear decrease in global mean precipitation, although further investigation is required to determine whether the loss of SSM/I on *F-14* around this time also contributes to the decrease.

The sensitivity of precipitation to changes in the observing system is investigated further in Fig. 20, which shows the evolution of the zonal-mean, monthly mean interannual anomalies of MERRA precipitation, together with the vertically integrated moisture increment from the analysis. Robertson et al. (2011) discuss these time series in detail. Except for the marked interannual variability in precipitation in the tropics associated with ENSO, there is close agreement between variations in the moisture increment and precipitation south of about 30°N. There is less similarity in the Northern Hemisphere where, presumably, the conventional data help to ameliorate changes associated with the satellite observations. Comparing Fig. 20 with Table 1 indicates that MERRA is sensitive to the SSM/I data. However, whereas

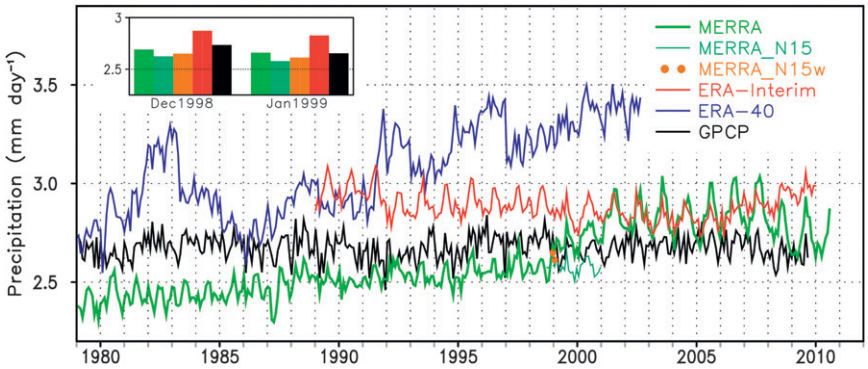

FIG. 19. Time series of global monthly mean precipitation (mm day^{-1}) for MERRA, ERA-Interim, and ERA-40, compared against GPCP. In addition to the time series from the MERRA distribution, two short data withholding experiments are shown. MERRA_N15 is from an experiment withholding all AMSU-A data from *NOAA-15*, and MERRA_N15w withholds only the AMSU-A window channels (1–3 and 15). For clarity, the inset shows the monthly mean values for December 1998 and January 1999.

SSM/I data tend to dry the atmosphere, AMSU-A data appear to have an overwhelming moistening effect almost everywhere.

Despite these issues, the fact that the global mean and all measures of the spatial distribution of precipitation in both MERRA and ERA-Interim are closer to the GPCP estimates than those of other reanalyses reflects the progress that has been made in representing the hydrologic cycle. However, given the given the relative magnitude of the analysis increment in the atmospheric water budget (discussed below) and of the remaining sensitivities to the observing system, we must conclude that even these reanalyses are not yet providing new information on precipitation variability, beyond what is available in the CMAP and GPCP products, and that they are particularly unsuitable to the study of trends.

b. *Analysis contributions to the water budget*

One of the important contributions from MERRA to water and energy budget studies is the careful attention paid to tracking all terms needed to close the budgets. All such terms are calculated inline during the assimilation cycle so as to produce an exactly closed budget. The terms include contributions from the analysis increments, and even (for example) the small "spurious" snow-related energy sources and sinks associated with several small accounting inconsistencies across the coupled land and atmospheric models. The budget terms are presented in the MERRA file specification document, as well as in B2011.

The size of the analysis increments is one measure of the quality of the system, especially in terms of bias. Ideally, the increments should be small and nonsystematic. Figure 21 shows the vertically integrated water vapor budget for January 2004. Clearly, the analysis increment is much smaller in amplitude and has smaller scale variability than the dominant terms in the budget: the atmospheric transport, precipitation, and evaporation. However, since the analysis increment is larger than the storage term (the total change in integrated water vapor over the month), it does make a nontrivial contribution to the overall budget.

c. *Precipitation impacts on land surface hydrology in MERRA*

Precipitation is the most important driver of land surface hydrological conditions, with an overwhelming

TABLE 1. Dates of observing system changes that appear to impact the global mean precipitation as seen in Fig. 19.

Date of data change	Data change
Jul 1987	SSM/I *F-8* introduced
Dec 1990	SSM/I *F-10* introduced
4 Dec 1991	SSM/I *F-8* not available
Dec 1991	SSM/I *F-11* introduced
May 1995	SSM/I *F-13* introduced
May 1997	SSM/I *F-14* introduced
13 Nov 1997	SSM/I *F-10* not available
Dec 1997	TMI rain rate introduced
Nov 1998	*N-15* AMSU-A introduced
Dec 1999	SSM/I *F-15* introduced
17 Dec 1999	SSM/I *F-11* not available
1 Jan 2001	*N-16* AMSU-A introduced
Oct 2002	EOS/*Aqua* AMSU-A introduced
1 Nov 2005	*N-18* AMSU-A introduced
25 Jul 2006	SSM/I *F-15* not available
4 Mar 2008	*N-16* AMSU-A not available
23 Aug 2008	SSM/I *F-14* not available
18 Nov 2009	SSM/I *F-13* not available

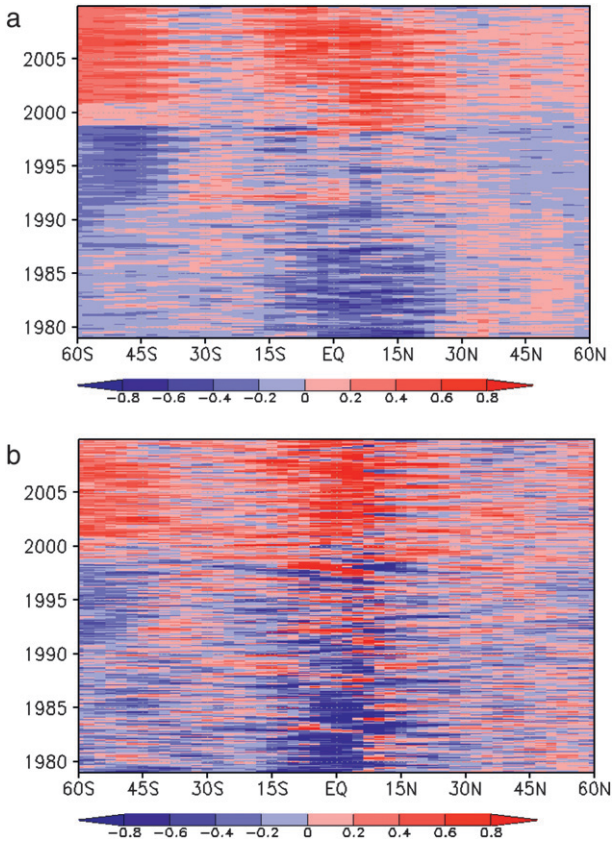

FIG. 20. Zonal-mean values of interannual anomalies of (a) vertically integrated moisture increments and (b) precipitation. Units for both quantities are mm day^{-1}. Anomalies are departures from climatological-mean seasonal cycles (see Robertson et al. 2011).

impact on the accuracy of simulated hydrological fields. Although the climatological distribution of MERRA precipitation is quite good, remaining biases in the long-term climatology and higher-frequency errors, particularly in the diurnal cycle, have a severe impact on the soil wetness estimates, as pointed out by R2011. They note three deficiencies in particular: (i) MERRA precipitation rates are less intense than observed and tend to appear as persistent drizzle; (ii) MERRA precipitation tends to be highest in the middle of the day, whereas the observations show frequent nighttime rain maxima; and (iii) MERRA incoming solar radiation during daytime precipitation events is not reduced as much as in the observations. Taken together, these three deficiencies lead to immediate reevaporation of much of the rainfall from droplets sitting on the surface of the vegetation canopy, which implies that not enough of the water is allowed to fall through the canopy and ultimately infiltrate the soil or contribute to surface runoff.

R2011 undertakes offline (land only) "MERRA-Land" simulations with two key changes: (i) the MERRA precipitation forcing is corrected by the pentad data from GPCP and (ii) some parameters of the Catchment model are modified to compensate for the precipitation deficiencies. Comparisons are then made with in situ observations and independent global data products to evaluate the land surface hydrology from MERRA and MERRA-Land estimates. The revised model parameters considerably improve the average interception loss ratio and contribute to more realistic latent heat fluxes in MERRA-Land. Generally, the skill levels of the MERRA and MERRA-Land estimates of soil moisture and runoff are comparable to those of ERA-Interim estimates. Moreover, snow depth and snow water equivalent compare well against in situ observations and the snow analysis from the Canadian Meteorological Center. Average anomaly correlation (R) skill levels for MERRA and MERRA-Land surface hydrological variables generally range from $R \sim 0.5$ to ~ 0.8, with the skill level of MERRA-Land being slightly higher (with statistical significance) than that of MERRA.

8. The stratosphere

As noted earlier, in addition to other applications, meteorological analyses produced by the GEOS DAS provide wind fields for transport studies by the stratospheric chemistry community. Hence, the quality of the analysis in the stratosphere is an important performance metric. In the Arctic lower stratosphere, the dominant components of the climate and variability were well represented in early analyses produced with low model tops (e.g., Pawson and Fiorino 1998a) since the large-scale structure in this region is well sampled by radiosondes. Even in the Antarctic, temperature retrievals from space-based data were adequate to constrain the polar vortex structure, but early analyses did not capture low temperatures characteristic of the polar regions. Increasing the height of the upper boundary led to substantial improvements in the analyzed structure of the middle stratosphere in ERA-40, ERA-Interim, and MERRA compared to the earlier products (P2011). These model improvements coupled with improved use of space-based radiance observations have led to consistent and accurate analyses of the middle and polar latitudes in both hemispheres, up to altitudes of 30–40 km. At higher levels, even the most recent analyses are less successful. Manney et al. (2008a,b) demonstrated that structures in the upper stratosphere and mesosphere are not well captured in analyses performed using systems that assimilate only nadir-sounding radiance observations, the dominant data type in the reanalyses.

In the tropics, the quasi-biennial oscillation (QBO) evident in the zonal-mean wind field has not always been

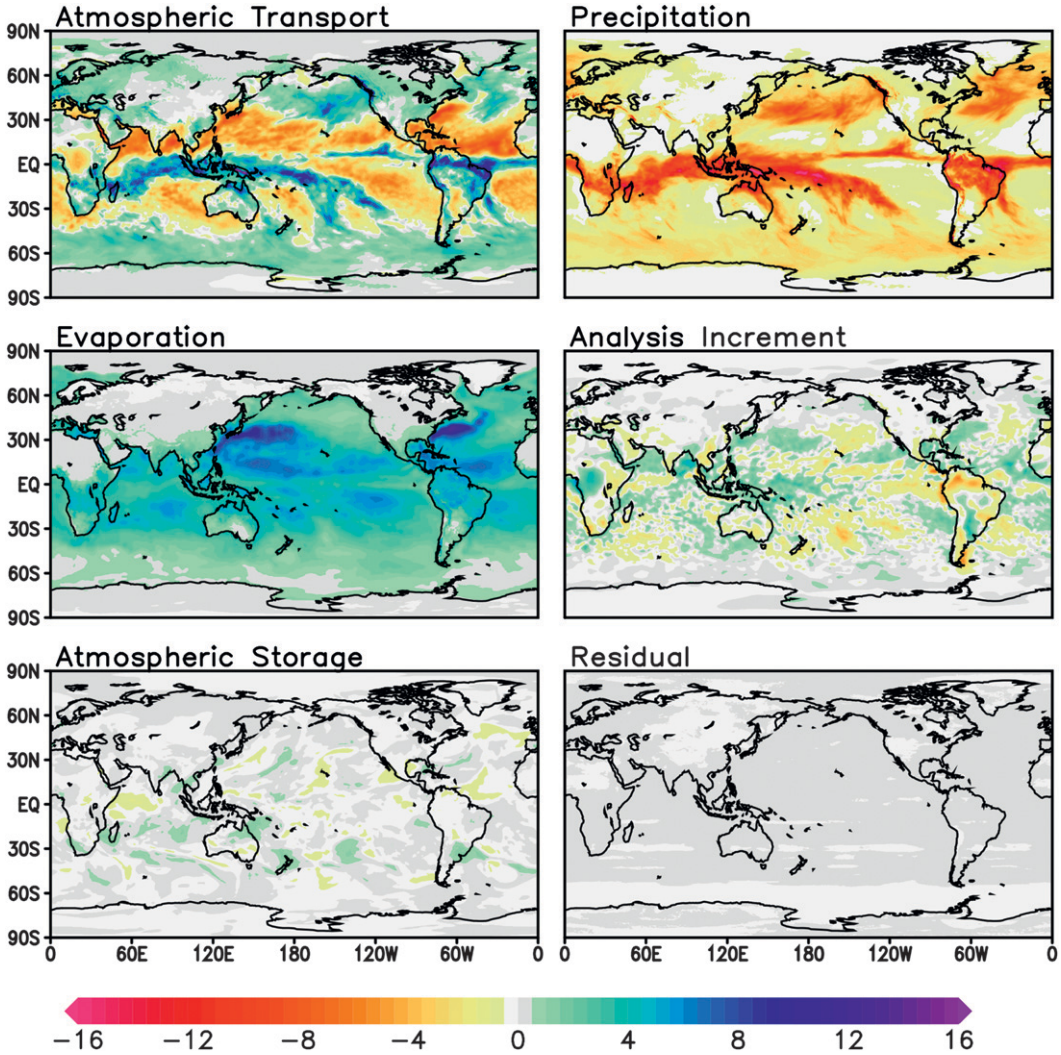

FIG. 21. MERRA's estimate of the vertically integrated water vapor budget for January 2004 (kg m^{-2} day^{-1}).

captured well in reanalyses. It was represented well by ERA-15 but not by NR1 (Pawson and Fiorino 1998b) or the earlier GEOS analyses. The reasons for this are not entirely clear, although Gaspari et al. (2006) showed that adequately long length scales are needed to spread wind information from sparse radiosondes around the globe, and that inadequate data selection can readily lead to good observations being rejected in favor of poor analyses in the tropical stratosphere. ERA-40 improved upon the representation in ERA-15 (Baldwin and Gray 2005) and now ERA-Interim analyses of the QBO are in excellent agreement with the observations. Figure 22 shows that MERRA too has realistic zonal wind variability in the lower stratosphere.

Zonal-mean winds in the tropical upper stratosphere are dominated by the semiannual oscillations (SAO), with transitions between easterly and westerly phases concentrated in shallow layers with large vertical shears (~10 m s^{-1} km^{-1}), which are associated with meridional curvature in the temperature field. The weak temperature gradients and the vertical averaging caused by the thick weighting functions associated with nadir radiance observations, as well as the lack of accurate balance constraints between winds and temperature fields in the tropics, mean that there is little observational constraint on the SAO winds in the reanalyses. It is thus not surprising that there are differences between the tropical upper-stratospheric winds from different reanalysis products (Fig. 22).

9. MERRA products and access

a. Products

A complete list of the analyzed and diagnosed fields produced by MERRA is given in the product file

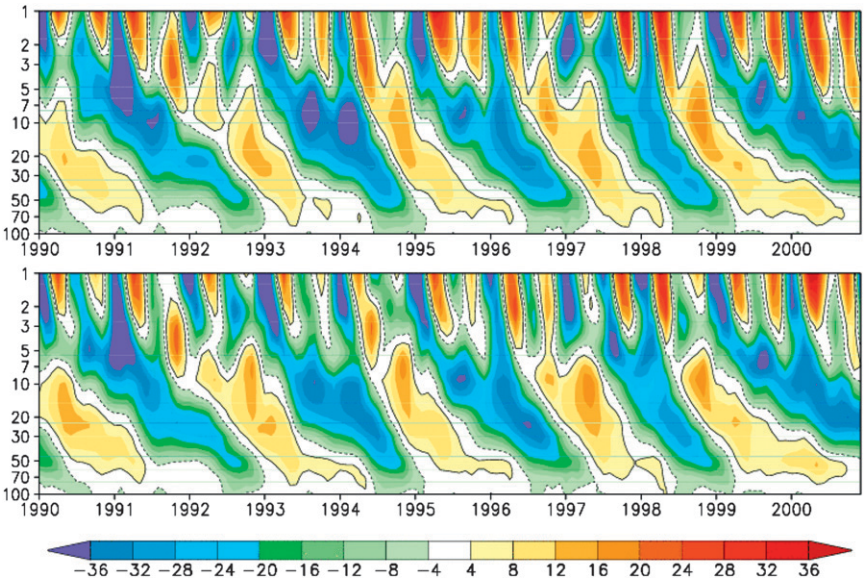

FIG. 22. Time series of the QBO and SAO as seen from the zonal-mean zonal wind component averaged between 10°S and 10°N in (top) MERRA and (bottom) ERA-Interim.

specification document available at the GMAO's MERRA Web site (http://gmao.gsfc.nasa.gov/merra/). A small advisory group helped to define the comprehensive set of enhanced postprocessed products that would be useful for supporting water and energy budget studies as well as chemical-transport modeling. The use of the IAU allows for higher-frequency products during the corrector segments depicted in Fig. 1 ("assimilation products") in addition to the traditional 6-hourly products that are generated directly from the analysis ("analyzed products").

There are two time-invariant and 24 time-varying product collections; some are on the model's native horizontal grid, ½° × ⅔°, and some are at reduced resolution, either 1° × 1.25° or 1.25° × 1.25°. A brief summary of products is provided in Table 2. Detailed information and a description of each variable are available in the MERRA file specification document. As mentioned earlier, MERRA provides closed atmospheric budgets, including the analysis increment terms. The observational forcing from the assimilation increments during the corrector segments is tallied in the output budgets of the model (e.g., water and enthalpy). Bosilovich et al. (2011) provides examples of the magnitudes of these terms in water and energy budgets.

b. Accessing MERRA data and information

The MERRA products are available online through the Goddard Earth Sciences Data and Information Services Center (GES DISC; http://disc.sci.gsfc.nasa.gov/daac-bin/DataHoldings.pl). Several different access options are available, including OPeNDAP and FTP. An FTP subsetter facilitates downloads of partial datasets. Online visualization options using the Giovanni Web-based application developed by the GES DISC (Acker and Leptoukh 2007) are also available. An online atlas of climatological information from MERRA, including comparisons with data-only products and other reanalyses, is being maintained (http://gmao.gsfc.nasa.gov/ref/merra/atlas/).

10. Summary and issues for the next generation of reanalyses

In most aspects, MERRA has achieved its primary goals of improving significantly on the previous generation of reanalyses in the representation of the atmospheric branch of the hydrological cycle and in providing complete information for budget studies. The availability of other updated reanalyses from ECMWF (ERA-Interim, 1988–present) and NCEP (CFSR, 1979–present) have provided a useful basis for evaluating MERRA and identifying common deficiencies that need to be addressed in the next generation of reanalyses.

Users of reanalysis data often request a characterization of the quality of and the uncertainty in the fields. While intercomparison with reference datasets is common practice for ascertaining quality, such comparisons are usually restricted to long-term climatological statistics and seldom provide state-dependent measures of the uncertainties involved. Ensemble assimilation methods, as used for the twentieth-century reanalysis based only on surface pressure observations (Compo et al. 2011), provide

TABLE 2. A summary of the MERRA product collections and their characteristics.

Collection type	No. of collections	Characteristics	Frequency
Invariants	2		
Analyzed fields	2	Native grid, instantaneous fields	6-hourly
[u, v, t, q, O_3, p]		Model and pressure level collections	
Assimilated fields	1	Reduced grid, instantaneous fields	3-hourly
		Pressure levels	
3D diagnostics	8	Reduced grid, time-averaged fields	3-hourly
		Pressure levels	
2D diagnostics	4	Native grid, time-averaged fields	Hourly
	1	Native grid, time-averaged land-related surface fields	Hourly
	1	Native grid, time-averaged ocean-related surface fields	Hourly
	1	Native grid, instantaneous vertical integrals	Hourly
Fields for offline Chemistry Transport Models	6	Various resolutions, grids, frequencies	

an inherent estimate of uncertainty albeit according to the model ensemble used. Comparison of such estimates with the statistics of differences between the most recent reanalyses using the full observing suite would be a useful undertaking. The innovations and analysis increments provide additional information on the quality of the analyses, as well as on the consistency of the different observations and how they are represented in the analysis. In addition to sharing observations, it would be useful for reanalysis producers to share such information on system performance in order to guide future development. The sharing of these and other metrics as part of future reanalyses would benefit users as well.

As suggested in sections 6–8, as model biases are reduced, assimilation increments are smaller and the differences in the climate variability from different reanalyses are reduced. However, there are still substantial differences between the existing reanalyses in poorly constrained quantities such as precipitation and surface fluxes due to differences in the assimilating models and in how the models interact with the assimilated data. These differences are an important measure of the uncertainty in reanalysis products. Observing system changes, which often manifest themselves in reanalysis time series by abrupt variations or discontinuities, can exacerbate such differences. These impacts from observing system changes must be distinguished from real climate variations and pose perhaps the greatest challenge for the next generation of reanalyses.

The performance of the reanalyses in the high stratosphere is also a cause for concern. A major issue is the lack of long-term in situ temperature observations, which, coupled with the model biases and the deep weighting functions of the SSU and AMSU-A radiance channels, makes it difficult to place precise constraints on the meteorological fields at these levels. It also makes the application of the variational bias correction of the observations inappropriate because of the major influence of model bias in the absence of other ''anchoring'' data. Future reanalyses will need to focus on improving models and better calibration of the input radiance data. Limb-sounding temperature data are available for certain periods, and may be used as anchors for a limited number of years, but these datasets generally do not overlap, so issues related to cross-dataset bias have not been addressed in detail. High quality temperature time series are available from occultation measurements, but the extremely low density of these data makes them unsuitable for assimilation. A more promising way of using them in reanalyses may be as calibration datasets—an aspect that will require substantial developments. Of course the availability of Global Positioning System Radio Occultation (GPS-RO) measurements is an important addition to the observing system from 2001 to the present. These were assimilated into ERA-Interim, but not into MERRA. Dee et al. (2011a) point out that these observations do not need to be bias corrected.

In spite of these challenges, significant improvements have come from each generation of reanalyses. Both the improvements and many of the remaining deficiencies are apparent in the time series of global-mean precipitation. Most of the improvements have come from the numerical weather prediction imperative, for which the assimilation systems will continue to evolve, taking advantage of new data types and improved methodologies. However, the question remains as to what might be done to improve reanalyses specifically, especially to address jumps and trends associated with changes in the observing system.

Thorne and Vose (2010) make some suggestions for how to undertake a climate reanalysis that will support trend analysis. Some of those suggestions—thinning the data to reduce shocks to the system, assimilating only long-term satellite observations, assimilating only raw data

(not bias-corrected or cross-calibrated data)—run counter to the experience of reanalysis developers to date (Dee et al. 2011b). For example, the different biases in MSU instruments from one satellite to the next (Zou et al. 2006) or in IR instruments (DU09) mean that there are no long-term *homogeneous* satellite observations, even from TOVS. Without careful bias correction, derived fields like precipitation are not adequate for climate variability studies, much less climate trend analysis. Nevertheless, for some applications, the reanalysis community needs to continue to seek ways to generate a climate analysis that minimizes the impacts of changes in the observing system while preserving the wealth of information gained as better observations are added. A workshop on improving observations for reanalysis (Schubert et al. 2006) recommended improvements to historical observations (including data mining), improved quality control, and further cross calibration and bias correction of observations to help to reduce the impacts from changes in the observing system. Continued interactions and collaborations between the producers of reanalyses, as well as with the data stewards, will be needed to make progress on these issues (Rienecker et al. 2011). In the meantime, the availability of three new reanalyses—MERRA, CFSR, and ERA-Interim—plus the anticipated availability of a new Japanese 55-yr Re-Analysis (JRA-55) provide researchers with a de facto ensemble of state-of-the-art climate analyses for making robust quality assessments and quantifying uncertainties.

Acknowledgments. The GEOS-5 AGCM and DAS development and the MERRA project in the Global Modeling and Assimilation Office were funded by NASA's Modeling, Analysis and Prediction program. That support is gratefully acknowledged. We thank Derek van Pelt for providing some of the figures for this paper, for assembling the online atlas, and for contributing to monitoring MERRA through the production phases. We thank the many others in the GMAO who contributed in various ways to the production and monitoring of MERRA. Dana Ostrenga, of the GES DISC, worked tirelessly with us to have MERRA distributed online. We gratefully acknowledge her contributions with those of her colleagues in the GES DISC. We thank Leopold Haimberger of the University of Vienna for generating new corrections with RAOBCORE V1.4 with the corrected Vaisala RS-80 sondes. Laurie Rokke contributed to the development of the radiative transfer module used for SSU. SSM/I data produced by Remote Sensing Systems were sponsored by the NASA Earth Science MEaSUREs DISCOVER project. Data are available online (www.remss.com). Support from the NASA Center for Climate Simulation (NCCS), providing a production environment for timely delivery of MERRA, was essential to the project. We thank the MERRA User Group who provided invaluable advice during the testing phase of MERRA, helped identify the product suites needed for a broad community of users, and then gave the final approval for production. The user group was Phil Arkin (chair, University of Maryland), Alan Betts (Atmospheric Research), Robert Black (Georgia Institute of Technology), David Bromwich (Ohio State University), John Roads (Scripps Institution of Oceanography), Jose Rodriguez (Goddard Space Flight Center), Steve Running (University of Montana), Paul Stackhouse Jr. (Langley Research Center), Kevin Trenberth (National Center for Atmospheric Research), and Glenn White (NOAA/NCEP). We also thank three anonymous reviewers whose comments helped clarify and improve the manuscript.

APPENDIX A

Acronyms and Their Definitions

3DVAR	Three-dimensional variational data assimilation
A-F	Analysis minus background (or first guess)
AGCM	Atmospheric general circulation model
AIREP	Aircraft report
AIRS	Advanced Infrared Sounder
AMI	Active Microwave Instrument
AMSU	Advanced Microwave Sounding Unit
Aqua	EOS P.M. satellite
ASDAR	Aircraft to Satellite Data Relay System
ATOVS	Advanced TIROS Operational Vertical Sounder
Aura	EOS CHEM satellite
BAS	British Antarctic Survey
BOM	Australian Bureau of Meteorology
CCARDS	Comprehensive Aerological Reference Dataset, Core Subset
CDAS	Climate Data Assimilation System
CERSAT	Center for Satellite Exploitation and Research
CFSR	Climate Forecast System Reanalysis
CMAP	Climate Prediction Center (CPC) Merged Analysis of Precipitation
CRTM	Community Radiative Transfer Model
DAS	Data Assimilation System
DOE	Department of Energy
ECMWF	European Centre for Medium-Range Weather Forecasts
EMC	NOAA/NCEP/Environmental Modeling Center
ENSO	El Niño–Southern Oscillation
EOS	Earth Observing System

ERA	ECMWF Re-Analysis
ERS-1, *-2*	*Environmental Research Satellites 1* and *2* (surface winds from AMI)
FGGE	First GARP Global Experiment
FTP	File transfer protocol
GARP	Global Atmospheric Research Program
GATE	GARP Atlantic Tropical Experiment
GEOS	Goddard Earth Observing System
GES DISC	Goddard Earth Sciences Data and Information Services Center
GMAO	Global Modeling and Assimilation Office
GMS	Geostationary Meteorological Satellite
GOCART	Goddard Chemistry, Aerosol, Radiation, and Transport
GOES	Geostationary Operational Environmental Satellite
GPCP	Global Precipitation Climatology Project
GPROF	Goddard profiling algorithm
GPS-RO	Global Positioning System Radio Occultation
GSFC	Goddard Space Flight Center
GSI	Gridpoint statistical interpolation
GTS	Global Telecommunication System
HALOE	Halogen Occultation Experiment
HIRS	High Resolution Infrared Radiation Sounder
IAU	Incremental Analysis Update
ICOADS	International Comprehensive Ocean–Atmosphere Dataset
IR	Infrared
JMA	Japan Meteorological Agency
JRA	Japanese Re-Analysis
LIE	Line Islands Experiment
MARS	Meteorological Archive and Retrieval System
MDCRS	Meteorological Data Collection and Reporting System
MERRA	Modern-Era Retrospective Analysis for Research and Applications
METAR	Routine aviation weather report
MIT	Massachusetts Institute of Technology
MLS	Microwave Limb Sounder
MODIS	Moderate Resolution Imaging Spectroradiometer
MSU	Microwave Sounding Unit
NASA	National Aeronautics and Space Administration
NCAR	National Center for Atmospheric Research
NCDC	National Climatic Data Center
NCEP	National Centers for Environmental Prediction
NESDIS	National Environmental Satellite, Data, and Information Service
NMC	National Meteorological Center
NOAA	National Oceanic and Atmospheric Administration
NR1	NCEP–NCAR reanalysis 1
NR2	NCEP–DOE reanalysis 2
O-A	Observation minus analysis
O-F	Observation minus background (or first guess)
OLR	Outgoing longwave radiation
OPeNDAP	Open-source Project for a Network Data Access Protocol
OPTRAN	Optical path transmittance
PAOBS	Synthetic surface pressure observation
PBL	Planetary boundary layer
PIBAL	Pilot balloon
QBO	Quasi-biennial oscillation
QuikSCAT	Quick Scatterometer
R1	NCEP–NCAR reanalysis
Raob	Radiosonde observation
RAOBCORE	Radiosonde Observation Bias Correction Using Reanalyses
RMS	Root mean square
RSS	Remote Sensing Systems
RTTOV	Radiative Transfer for TIROS Operational Vertical Sounder
SAO	Semiannual oscillation
SBUV/2	Solar Backscatter Ultraviolet Spectral Radiometer-2
SNO	Simultaneous nadir overpass
SSM/I	Special Sensor Microwave Imager
SSU	Stratospheric Sounding Unit
TCWV	Total-column water vapor
TD	Tape Deck
Terra	EOS A.M. satellite
TIROS	Television and Infrared Observatory Spacecraft
TMI	TRMM Microwave Imager
TOVS	TIROS Operational Vertical Sounder
TRMM	Tropical Rainfall Measuring Mission
TSR	Time series raob (NCAR format for upper-air data)
USAF	U.S. Air Force
USCNTRL	U.S. controlled ocean weather stations
UTC	Coordinated universal time
VBC	Variational bias correction

APPENDIX B

Observations Used in MERRA Production

TABLE B1. Conventional data in MERRA, availability and data sources.

Data source/type	Period	Data supplier
Raobs/pibals/drops	1970–present	See Table B2
Wind profiles	14 May 1992–present	NCEP CDAS
Conventional, ASDAR, and MDCRS aircraft reports	1970–present	NCEP, ECMWF
Paobs	1978–17 Aug 2010	NCEP, ECMWF, JMA, BOM
GMS, Meteosat, IR and visible winds	1977–present	NCEP, JMA
GOES cloud drift winds	1978–present	NCEP
EOS/*Terra*/MODIS winds	1 Jul 2002–present	NCEP
EOS/*Aqua*/MODIS winds	1 Sep 2003–present	NCEP
Surface land observations	1970–present	NCEP
Surface ship and buoy observations	1970–present	ICOADS
SSM/I rain rate, GPROF algorithm (Kummerow et al. 2001)	Jul 1987–present	NASA/GES DISC
SSM/I V6 wind speed (Wentz, 1997)	Jul 1987–present	RSS
TMI rain rate	Dec 1997–present	NASA/GES DISC
QuikSCAT surface winds	Jul 1999–present	Jet Propulsion Laboratory
ERS-1 surface winds	5 Aug 1991–21 May 1996	CERSAT
ERS-2 surface winds	19 Mar 1996–17 Jan 2001	CERSAT
SBUV2 ozone (version 8 retrievals)	Oct 1978–present	NASA/GES DISC

TABLE B2. Historical radiosonde, dropsonde, and PIBAL archive sources.

NCEP–NCAR	Office Note 20, Office Note 29, NMC/NCEP/GTS ingest
ECMWF	ECMWF/FGGE, ECMWF/MARS/GTS ingest
JMA	Japan Meteorological Agency GTS ingest
NCAR	International archives: Argentina, Australia, Brazil, Canada, China, Dominica, France, India, Japan, NCDC, New Zealand, Russia, Singapore, South Africa, United Kingdom
	Research sets: PermShips, RemoteSites, Ptarmigan, Scherhaug, LIE, GATE, BAS
NCDC	U.S. military and academic sources: TD52, TD53, TD54, TD90, USCNTRL, USAF, U.S. Navy, CCARDS, MIT

TABLE B3. Satellite radiance data in MERRA, availability and data sources.

Data source/type	Period	Data supplier
TOVS/tn (TIROS N)	30 Oct 1978–1 June 1980	NCAR
TOVS/na (*NOAA-6*)	2 Jul 1979–17 Apr 1983	NCAR
TOVS/nc (*NOAA-7*)	11 Jul 1981–1 Jun 1986	NCAR
TOVS/ne (*NOAA-8*)	26 Apr 1983–1 Jan 1985	NCAR
TOVS/nf (*NOAA-9*)	1 Jan 1985–1 Nov 1988	NESDIS, NCAR
TOVS/ng (*NOAA-10*)	25 Nov 1986–17 Sep 1991	NESDIS, NCAR
TOVS/nh (*NOAA-11*)	2 Sep 1988–31 Dec 1994	NESDIS, NCAR
TOVS/nd (*NOAA-12*)	18 Aug 1991–14 Jul 1997	NESDIS, NCAR
TOVS/nj (*NOAA-14*)	19 Jan 1995–10 Oct 2006	NESDIS
TOVS/nk (*NOAA-15*)	1 Jul 1998–present	NESDIS
TOVS/nl (*NOAA-16*)	2 Mar 2001–present	NESDIS
TOVS/nm (*NOAA-17*)	1 Mar 2003–present	NESDIS
TOVS/nn (*NOAA-18*)	5 Oct 2005–present	NESDIS
EOS/*Aqua*	Oct 2002–present	NESDIS
SSM/I V6 (*F-8*)	Jul 1987–4 Dec 1991	RSS
SSM/I V6 (*F-10*)	Dec 1990–13 Nov 1997	RSS
SSM/I V6 (*F-11*)	Dec 1991–17 Dec 1999	RSS
SSM/I V6 (*F-13*)	May 1995–18 Nov 2009	RSS
SSM/I V6 (*F-14*)	May 1997–23 Aug 2008	RSS
SSM/I V6 (*F-15*)	Dec 1999–25 Jul 2006	RSS
GOES sounder	Jan 2001–3 Dec 2007	NCEP
SBUV2 ozone (version 8 retrievals)	Oct 1978–present	GES DISC

REFERENCES

Acker, J. G., and G. Leptoukh, 2007: Online analysis enhances use of NASA Earth science data. *EOS, Trans. Amer. Geophys. Union,* **88** (2), 14–17.

Adler, R. F., and Coauthors, 2003: The version-2 Global Precipitation Cimatology Project (GPCP) monthly precipitation analysis (1979–present). *J. Hydrometeor.,* **4,** 1147–1167.

Alishouse, J. C., S. A. Snyder, V. Jennifer, and R. R. Ferraro, 1990: Determination of oceanic total precipitable water from the SSM/I. *IEEE Trans. Geosci. Remote Sens.,* **28,** 811–816.

Bacmeister, J. T., M. J. Suarez, and F. R. Robertson, 2006: Rain reevaporation, boundary layer–convection interactions, and Pacific rainfall patterns in an AGCM. *J. Atmos. Sci.,* **63,** 3383–3403.

Baldwin, M. P., and L. J. Gray, 2005: Tropical stratospheric zonal winds in ECMWF ERA-40 reanalysis, rocketsonde data, and rawinsonde data. *Geophys. Res. Lett.,* **32,** L09806, doi:10.1029/2004GL022328.

Ballish, B. A., and V. K. Kumar, 2008: Systematic differences in aircraft and radiosonde temperatures: Implications for NWP and climate studies. *Bull. Amer. Meteor. Soc.,* **89,** 1689–1707.

Bloom, S., L. Takacs, A. DaSilva, and D. Ledvina, 1996: Data assimilation using incremental analysis updates. *Mon. Wea. Rev.,* **124,** 1256–1271.

Bosilovich, M. G., F. R. Robertson, and J. Chen, 2011: Global energy and water budgets in MERRA. *J. Climate,* in press.

Bromwich, D. H., and S.-H. Wang, 2005: Evaluation of the NCEP–NCAR and ECMWF 15- and 40-yr reanalyses using rawinsonde data from two independent Arctic field experiments. *Mon. Wea. Rev.,* **133,** 3562–3578.

Brunke, M., Z. Wang, X. Zeng, M. Bosilovich, and C.-L. Shie, 2011: An assessment of the uncertainties in ocean surface turbulent fluxes in 11 reanalysis, satellite-derived, and combined global datasets. *J. Climate,* in press.

Cardinali, C., L. Isaksen, and E. Anderson, 2003: Use and impact of automated aircraft data in a global 4DVAR data assimilation system. *Mon. Wea. Rev.,* **131,** 1865–1877.

Chen, Y., Y. Han, P. Van Delst, and F. Weng, 2010: On water vapor Jacobian in fast radiative transfer model. *J. Geophys. Res.,* **115,** D12303, doi:10.1029/2009JD013379.

Chou, M.-D., and M. J. Suarez, 1999: A solar radiation parameterization for atmospheric studies. NASA Tech. Rep. Series on Global Modeling and Data Assimilation, NASA/TM-1999-104606, Vol. 15, 40 pp.

——, ——, X. Z. Liang, and M.M.-H. Yan, 2001: A thermal infrared radiation parameterization for atmospheric studies. NASA Tech. Rep. Series on Global Modeling and Data Assimilation, NASA/TM-2001-104606, Vol. 19, 56 pp.

Colarco, P. R., A. da Silva, M. Chin, and T. Diehl, 2010: Global aerosol distributions in the NASA GEOS-4 model and comparisons to satellite and ground-based aerosol optical depth. *J. Geophys. Res.,* **115,** D14207, doi:10.1029/2009JD012820.

Collins, W., 1999: Determination of new adjustment tables in order to bring radiosonde temperature and height measurements from different sonde types into relative agreement. EMC/NCEP/NOAA, 12 pp. [Available online at http://www.emc.ncep.noaa.gov/mmb/papers/collins/new_tables/new_tables.html.]

Compo, G. P., and Coauthors, 2011: The Twentieth Century Reanalysis Project. *Quart. J. Roy. Meteor. Soc.,* **137,** 1–28.

Cullather, R. I., and M. G. Bosilovich, 2011: The moisture budget of the polar atmosphere in MERRA. *J. Climate,* **24,** 2861–2879.

Dee, D., 2005: Bias and data assimilation. *Quart. J. Roy. Meteor. Soc.,* **131,** 3323–3343.

——, and A. M. da Silva, 1999: Maximum-likelihood estimation of forecast and observation error covariance parameters. Part I: Methodology. *Mon. Wea. Rev.,* **127,** 1822–1834.

——, and S. Uppala, 2008: Variational bias correction in ERA-Interim. ECMWF Tech. Memo. 575, ECMWF, Reading, United Kingdom, 26 pp.

——, and ——, 2009: Variational bias correction of satellite radiance data in the ERA-Interim reanalysis. *Quart. J. Roy. Meteor. Soc.,* **135,** 1830–1841.

——, and Coauthors, 2011a: The ERA-Interim reanalysis: Configuration and performance of the data assimilation system. *Quart. J. Roy. Meteor. Soc.,* **137,** 553–597.

——, E. Källén, A. J. Simmons, and L. Haimberger, 2011b: Comments on ''Reanalyses suitable for characterizing long-term trends.'' *Bull. Amer. Meteor. Soc.,* **92,** 70–72.

Derber, J. C., and W.-S. Wu, 1998: The use of TOVS cloud-cleared radiances in the NCEP SSI analysis system. *Mon. Wea. Rev.,* **126,** 2287–2299.

——, R. J. Purser, W.-S. Wu, R. Treadon, M. Pondeca, D. Parrish, and D. Kleist, 2003: Flow-dependent Jb in a global grid-point 3DVAR. *Proc. ECMWF Annual Seminar on Recent Developments in Data Assimilation for Atmosphere and Ocean,* Reading, United Kingdom, ECMWF, 125–134.

Desroziers, G., L. Berre, B. Chapnik, and P. Poli, 2005: Diagnosis of observation, background and analysis-error statistics in observation space. *Quart. J. Roy. Meteor. Soc.,* **131,** 3385–3396.

Ferraro, R. R., N. C. Grody, F. Weng, and A. Basist, 1996: An eight-year (1987–94) time series of rainfall, clouds, water vapor, snow cover, and sea ice derived from SSM/I measurements. *Bull. Amer. Meteor. Soc.,* **77,** 891–905.

Garcia, R. R., and B. A. Boville, 1994: Downward control of the mean meridional circulation and temperature distribution of the polar winter stratosphere. *J. Atmos. Sci.,* **51,** 2238–2245.

Gaspari, G., S. E. Cohn, J. Guo, and S. Pawson, 2006: Construction and application of covariance functions with variable length fields. *Quart. J. Roy. Meteor. Soc.,* **132,** 1815–1838.

Haimberger, L., 2007: Homogenization of radiosonde temperature time series using innovation statistics. *J. Climate,* **20,** 1377–1403.

Han, Y., P. van Delst, Q. Liu, F. Weng, B. Yan, R. Treadon, and J. Derber, 2006: JCSDA Community Radiative Transfer Model (CRTM)—Version 1. NOAA Tech. Rep. 122, 33 pp.

Harnik, N., J. Perlwitz, and T. A. Shaw, 2011: Observed decadal changes in downward wave coupling between the stratosphere and troposphere in the Southern Hemisphere. *J. Climate,* in press.

Hollingsworth, A., and P. Lönnberg, 1989: The verification of objective analyses: Diagnostics of analysis system performance. *Meteor. Atmos. Phys.,* **40,** 3–27.

Kalnay, E., and Coauthors, 1996: The NCEP/NCAR 40-Year Reanalysis Project. *Bull. Amer. Meteor. Soc.,* **77,** 437–471.

Kistler, R., and Coauthors, 2001: The NCEP–NCAR 50-Year Reanalysis: Monthly means CD-ROM and documentation. *Bull. Amer. Meteor. Soc.,* **82,** 247–267.

Kobayashi, S., M. Matricardi, D. Dee, and S. Uppala, 2009: Toward a consistent reanalysis of the upper stratosphere based on radiance measurements from SSU and AMSU-A. *Quart. J. Roy. Meteor. Soc.,* **135,** 2086–2099.

Koster, R. D., M. J. Suárez, A. Ducharne, M. Stieglitz, and P. Kumar, 2000: A catchment-based approach to modeling land surface processes in a GCM, Part 1, Model structure. *J. Geophys. Res.,* **105,** 24 809–24 822.

Kummerow, C., and Coauthors, 2001: The evolution of the Goddard Profiling Algorithm (GPROF) for rainfall estimation from passive microwave sensors. *J. Appl. Meteor.,* **40,** 1801–1820.

Lin, S.-J., 2004: A vertically Lagrangian finite-volume dynamical core for global models. *Mon. Wea. Rev.,* **132,** 2293–2307.

Lock, A. P., A. R. Brown, M. R. Bush, G. M. Martin, and R. N. B. Smith, 2000: A new boundary layer mixing scheme. Part I: Scheme description and single-column model tests. *Mon. Wea. Rev.,* **138,** 3187–3199.

Louis, J., M. Tiedtke, and J. Geleyn, 1982: A short history of the PBL parameterization at ECMWF. *Proc. ECMWF Workshop on Planetary Boundary Layer Parameterization,* Reading, United Kingdom, ECMWF, 59–80.

Manney, G. L., and Coauthors, 2008a: The evolution of the stratopause during the 2006 major warming: Satellite data and assimilated meteorological analyses. *J. Geophys. Res.,* **113,** D11115, doi:10.1029/2007JD009097.

——, and Coauthors, 2008b: The high Arctic in extreme winters: Vortex, temperature, and MLS and ACE-FTS trace gas evolution. *Atmos. Chem. Phys.,* **8,** 505–522.

McFarlane, N. A., 1987: The effect of orographically excited gravity wave drag on the general circulation of the lower stratosphere and troposphere. *J. Atmos. Sci.,* **44,** 1775–1800.

McMillin, L. M., X. Xiong, Y. Han, T. J. Kleespies, and P. Van Delst, 2006: Atmospheric transmittance of an absorbing gas. 7. Further improvements to the OPTRAN 6 approach. *Appl. Opt.,* **45,** 2028–2034, doi:10.1364/AO.45.002028.

Moorthi, S., and M. J. Suarez, 1992: Relaxed Arakawa–Schubert, a parameterization of moist convection for general circulation models. *Mon. Wea. Rev.,* **120,** 978–1002.

Onogi, K., and Coauthors, 2005: JRA-25: Japanese 25-Year Re-Analysis Project—Progress and status. *Quart. J. Roy. Meteor. Soc.,* **131,** 3259–3268.

Pawson, S., and M. Fiorino, 1998a: The tropical lower stratosphere in atmospheric reanalyses. Part 1: Thermal structure and the annual cycle. *Climate Dyn.,* **14,** 631–644.

——, and ——, 1998b: The tropical lower stratosphere in atmospheric reanalyses. Part 2: The quasi-biennial oscillation. *Climate Dyn.,* **14,** 645–658.

——, and Coauthors, 2007: Stratospheric transport using six-hour averaged winds from a data assimilation system. *J. Geophys. Res.,* **112,** D23103, doi:10.1029/2006JD007673.

Purser, R. J., W.-S. Wu, D. F. Parrish, and N. M. Roberts, 2003a: Numerical aspects of the application of recursive filters to variational statistical analysis. Part I: Spatially homogeneous and isotropic Gaussian covariances. *Mon. Wea. Rev.,* **131,** 1524–1535.

——, ——, ——, and ——, 2003b: Numerical aspects of the application of recursive filters to variational statistical analysis. Part II: Spatially inhomogeneous and anisotropic general covariances. *Mon. Wea. Rev.,* **131,** 1536–1548.

Randel, W. J., F. Wu, J. M. Russell, A. Roche, and J. W. Waters, 1998: Seasonal cycles and QBO variations in stratospheric CH_4 and H_2O observed in UARS HALOE data. *J. Atmos. Sci.,* **55,** 163–185.

Redder, C. R., J. K. Luers, and R. E. Eskridge, 2004: Unexplained discontinuity in the U.S. radiosonde temperature data. Part II: Stratosphere. *J. Atmos. Oceanic Technol.,* **21,** 1133–1144.

Reynolds, R. W., N. A. Rayner, T. M. Smith, D. C. Stokes, and W. Wang, 2002: An improved in situ and satellite SST analysis for climate. *J. Climate,* **15,** 1609–1625.

Rienecker, M. M., and Coauthors, 2008: The GEOS-5 Data Assimilation System—Documentation of versions 5.0.1 and 5.1.0, and 5.2.0. NASA Tech. Rep. Series on Global Modeling and Data Assimilation, NASA/TM-2008-104606, Vol. 27, 92 pp.

——, and Coauthors, 2011: Atmospheric reanalyses: Recent progress and prospects for the future. NASA/TM-2011-104606, Vol. 29, NASA GSFC, 35 pp.

Robertson, F. R., M. G. Bosilovich, J. Chen, and T. L. Miller, 2011: The effect of satellite observing system changes on MERRA water and energy fluxes. *J. Climate,* in press.

Saha, S., and Coauthors, 2010: The NCEP Climate Forecast System Reanalysis. *Bull. Amer. Meteor. Soc.,* **91,** 1015–1057.

Saunders, R., and Coauthors, 2007: A comparison of radiative transfer models for simulating Atmospheric Infrared Sounder (AIRS) radiances. *J. Geophys. Res.,* **112,** D01S90, doi:10.1029/2006JD007088.

Schubert, S. D., R. Rood, and J. Pfaendtner, 1993: An assimilated dataset for earth science applications. *Bull. Amer. Meteor. Soc.,* **74,** 2331–2342.

——, D. Dee, S. Uppala, J. Woollen, J. Bates, and S. Worley, 2006: Workshop report: The development of improved observational datasets for reanalysis: Lessons learned and future directions. NOAA/NASA–NSF, 31 pp. [Available online at http://gmao.gsfc.nasa.gov/pubs/docs/Schubert273.pdf.]

——, H. Wang, and M. J. Suarez, 2011: Warm season subseasonal variability and climate extremes in the Northern Hemisphere: The role of stationary Rossby waves. *J. Climate,* in press.

Shine, K. P., J. J. Barnett, and W. J. Randel, 2008: Temperature trends derived from Stratospheric Sounding Unit radiances: The effect of increasing CO_2 on the weighting function. *Geophys. Res. Lett.,* **35,** L02710, doi:10.1029/2007GL032218.

Thorne, P. W., and R. S. Vose, 2010: Reanalyses suitable for characterizing long-term trends: Are they really achievable? *Bull. Amer. Meteor. Soc.,* **91,** 353–361.

Treadon, R. E., H.-L. Pan, W.-S. Wu, Y. Lin, W. S. Olson, and R. J. Kuligowski, 2002: Global and Regional Moisture Analyses at NCEP. *Proc. ECMWF/GEWEX Workshop on Humidity Analysis,* Reading, United Kingdom, ECMWF, 33–47.

Uppala, S. M., and Coauthors, 2005: The ERA-40 Re-Analysis. *Quart. J. Roy. Meteor. Soc.,* **131,** 2961–3012.

Wentz, F. J., 1997: A well-calibrated ocean algorithm for SSM/I. *J. Geophys. Res.,* **102,** 8703–8718.

Wu, W.-S., R. J. Purser, and D. F. Parrish, 2002: Three-dimensional variational analysis with spatially inhomogeneous covariances. *Mon. Wea. Rev.,* **130,** 2905–2916.

Xie, P., and P. A. Arkin, 1996: Global precipitation: A 17-year monthly analysis based on gauge observations, satellite estimates, and numerical model outputs. *Bull. Amer. Meteor. Soc.,* **78,** 2539–2558.

Yi, Y., J. S. Kimball, L. A. Jones, R. H. Reichle, and K. C. McDonald, 2011: Evaluation of MERRA land surface estimates in preparation for the Soil Moisture Active Passive mission. *J. Climate,* in press.

Zou, C., M. D. Goldberg, Z. Cheng, N. C. Grody, J. T. Sullivan, C. Cao, and D. Tarpley, 2006: Recalibration of microwave sounding unit for climate studies using simultaneous nadir overpasses. *J. Geophys. Res.,* **111,** D19114, doi:10.1029/2005JD006798.